Creating Ultrahigh Intensities Using a Passive Enhancement Cavity

by

Thomas John Hammond

B.Sc., The University of Winnipeg, 2003

A THESIS SUBMITTED IN PARTIAL FULFILMENT OF
THE REQUIREMENTS FOR THE DEGREE OF

Master of Science

in

The Faculty of Graduate Studies

(Physics)

The University Of British Columbia

April, 2007

Abstract

A table-top source for coherent extreme ultraviolet (EUV) radiation is beneficial for spectroscopic techniques requiring photon energies of more than a few electron volts. Other systems which can produce the required photon flux and photon energies are large and have limited beam time such as the Canadian Light Source or a free-electron laser. Conversely, conventional optics (lasers and crystals) cannot produce such high photon energies. An alternative method uses high harmonic generation, a technique that requires high intensities ($> 10^{13} W/cm^2$). The high-order harmonics that are created retain temporal and spatial coherence, yet are now in the ultraviolet and soft X-ray region of the electromagnetic spectrum. The goal of this thesis was to design an optical source and amplifier system that created intensities which surpassed the threshold required for high harmonic generation. The approach used kept the bandwidth narrow and allowed for high EUV photon flux, useful for spectroscopy. Towards this end, a titanium-doped sapphire laser oscillator was designed and built to output $> 1W$ average power, with a peak power $> 100kW$ but limited in bandwidth to $2nm$. The methods for obtaining such a high peak power - yet in a stable, bandwidth limited case - are presented. The laser output was then injected into an enhancement cavity with a high Q factor, increasing the average power by a factor of 50. The peak intensity has reached $4 \times 10^{12} W/cm^2$, or to within a factor of 2 of the threshold required to create EUV radiation. Lastly, methods for coupling out the EUV from the enhancement cavity are presented.

Table of Contents

Abstract ii

Table of Contents iii

List of Tables v

List of Figures vi

Chapter 1 Introduction 1

Chapter 2 Background and Theory 4

2.1 The Laser Oscillator 6

2.1.1 Gain Medium: the Titanium Sapphire Crystal 6

2.1.2 Lasing and Modelocking 7

2.1.3 Limiting the Bandwidth 10

2.1.4 Dispersion Compensation 14

2.1.5 Laser Cavity Extension via Unity Transform 19

2.1.6 The ABCD Matrix 22

2.1.7 Cavity Extension 23

2.2 Enhancement Cavity 25

2.2.1 Intensity Enhancement 26

2.2.2 Modematching 35

2.2.3 Diffraction inside a Resonator 37

2.3 Locking the Laser Oscillator to the Enhancement Cavity 42

2.4 High-Order Harmonic Generation 47

Chapter 3 Results and Discussion 50

3.1 The Ti:Sapphire Oscillator Setup 50

3.1.1 Thermal Lensing 50

3.1.2 The Extended Cavity 51

3.1.3 Dispersion Compensation 52

3.1.4 Active Control of the Laser Cavity 53

3.2 Beam Profile Measurement and Modematching 56

3.3 The Enhancement Cavity 58

3.3.1 Setup of the Enhancement Cavity 58

3.3.2 Alignment of the Enhancement Cavity 58

3.3.3 Measurement of the Enhancement Cavity Finesse 60

3.3.4 Current Enhancement Cavity Buildup Results 61

Chapter 4 Conclusions and Future Work 64

Bibliography 66

Appendix A The Ti:Sapphire Laser 70

Appendix B Approximation of d/a 72

Appendix C Codes 73

C.1 Unity Transform Mirror Calculation 73

C.2 Beam Characterization and Guiding to the EC 75

C.2.1 Beam Profile Measurement 75

C.2.2 Modematching 76

C.3 Diffraction Within a Resonator 82

List of Tables

2.1 Table of materials used in the oscillator and their group velocity and delay dispersion values; c is the speed of light; M_i represents one of the 4 mirrors that are dispersion compensated. Numbers are for single pass through the optic element. 17

2.2 Gaussian beam parameters taken from [10] 21

List of Figures

2.1 Source schematic . . . 5

2.2 Frequency comb . . . 8

2.3 Limiting bandwidth via prism . . . 11

2.4 Prism dispersion . . . 12

2.5 Supported bandwidth . . . 13

2.6 A chirped pulse . . . 17

2.7 Prism pair configurations . . . 19

2.8 A ray propagating in direction $\vec{k}$ through space. The slope of the beam relative to the z axis is typically small such that $\tan\theta \approx \sin\theta \approx \theta$. . . . 20

2.9 The extended cavity schematic . . . 24

2.10 The field inside a cavity . . . 27

2.11 The intracavity intensity as a function of the input coupler and phase . . . 28

2.12 The modes of a cavity . . . 29

2.13 Mode alignment . . . 30

2.14 Broad bandwidth enhancement function . . . 32

2.15 A schematic of modematching . . . 36

2.16 Beam divergence for HHG . . . 38

2.17 Cavity ray trace . . . 39

2.18 Linear resonator geometry . . . 40

2.19 Resonator eigenmode algorithm 42
2.20 Schematic of Hänsch locking technique 43
2.21 Error signal for multimode EC 45
2.22 Measured error signal 46
2.23 Maximum error drift 47
2.24 Electron in electric fields 48

3.1 Schematic of $25MHz$ Ti:Sapphire laser 51
3.2 The Ti:Sapphire laser output spectrum and autocorrelation trace 53
3.3 Pulse train and Microwave spectrum 54
3.4 Vibration noise on spectrum 55
3.5 The beam profile 56
3.6 A gaussian fit to beam profile 58
3.7 Schematic of the EC 59
3.8 Cavity ring-down signal 62
3.9 High finesse ringdown 62

A.1 The Ti:Sapphire laser 70
A.2 Ti:Sapph crystal mount 71

B.1 Small R limits for approximations 72

C.1 Ring cavity and its similar linear cavity 83
C.2 Beam profile in a confocal resonator 85
C.3 Beam profile from Fox-Li method 86

Chapter 1

Introduction

With the development of dye lasers and the Titanium Sapphire ($Ti{:}Al_2O_3$) laser, coherent light in the optical region and near infrared (700 – 1100nm) is now easily accessible. Using second or third harmonic generation (SHG and THG respectively), these sources can be extended to the ultraviolet ($100nm <$ UV $< 400nm$). Unfortunately, realising a coherent source at even shorter wavelengths becomes increasingly difficult since the crystals typically used for harmonic generation begin to absorb in the UV. As an alternative, using the nonlinear response of a dilute noble gas allows for the creation of high-order harmonics extending beyond the ultraviolet region. High-order harmonic generation (HHG) has become a leading method of creating coherent light in the extreme ultraviolet (EUV) and the X-ray regions [1] from an optical source.

The coherent EUV radiation produced by HHG is through a nonlinear process which requires the electromagnetic field of an external light source to be comparable with the Coulomb potential within an atom. This translates to an intensity of a fundamental optical beam greater than $10^{13}W/cm^2$. To this end, we will be concerned with the peak power of the laser in order to generate the EUV. A higher peak power can be more easily attained using shorter pulses, which translates to more efficient EUV production. However, a shorter pulse requires a broader bandwidth from the fundamental (laser oscillator), which translates into a broader bandwidth for the EUV. The majority of current research on HHG is to produce the highest possible harmonic, typically using ultrashort (femtosecond) pulses ($1fs = 10^{-15}s$). Much of the research has involved the development of better regenerative and multipass amplifiers and (quasi) phase-matching for more efficient high harmonic production [1, 2]. These refinements have led to harmonics on the order of several hundred, reaching energies of greater than $250eV$ (or $< 5nm$). Although some of the first lasers used in HHG had picosecond ($1ps = 10^{-12}s$) pulse duration [3], current work has focused almost exclusively on shorter pulses since the peak power is higher and the pulse duration of the resulting EUV pulses has entered the attosecond ($1as = 10^{-18}s$) regime [4]. Since these systems use regenerative or multipass amplifiers, they have low repetition rates (from a few Hertz to kHz), which means that although they can produce much higher pulse energies they consequently have a low photon flux. The limitation on the repetition rate is due to the gain dynamics in the amplifier system which has lead to interest in amplification schemes without traditional gain media, such as passive enhancement cavities.

An enhancement cavity uses a low loss (high finesse) design to trap light. As the cavity is pumped with a fundamental radiation field, the light travels within the cavity and constructive interference from multiple passes acts as a passive amplification scheme. This mechanism requires that the light is still coherent. The intracavity power increases by a few orders of magnitude, and when the input light is from a pulsed oscillator, the repetition rate of the enhancement cavity can be the same as that of the laser oscillator (tens to hundreds of megahertz). This high repetition rate is the advantage of the passive enhancement cavity over multipass/regenerative amplifiers because of the high flux of EUV that can be created. Recent work using an enhancement cavity has enabled the creation of high harmonics at 100MHz repetition rates [5, 6]. This work has led to harmonic generation reaching sub-$100nm$ wavelength light. However, in order to reach the intensity threshold for harmonic generation, these pulses are required to be sub-$50fs$, implying a bandwidth of at least $20nm$.

The goal of this project is to create high flux (greater than 10^{10} photons/sec) EUV light with narrow bandwidth ($E/\Delta E > 5000$ where E is the photon energy and ΔE is the energy width). One reason for these design considerations is for a potential application which is to replace the radiation from a synchrotron with a tabletop laser source for Angle Resolved PhotoEmission Spectroscopy (ARPES). Since a constraint of our work is that the high harmonic is to be of narrow bandwidth, there is a minimum limit to the optical (fundamental or driving) pulse duration. Therefore, by balancing these competing characteristics of high flux, high photon energy, and high spectral purity, our EUV table-top source can be modified for each potential application. For example, ARPES requires high spectral purity and can tolerate low photon flux, whereas X-ray imaging needs a high photon flux, but is not limited by the energy resolution. This thesis describes the setup of a high repetition rate laser capable of generating relatively narrow bandwidth, picosecond pulses, yet reaching the threshold intensity required for HHG.

Chapter 2

Background and Theory

As will be demonstrated, the output intensity of a standard table-top oscillator is insufficient to reach the threshold for HHG. In order to balance the competing factors that are outlined in Chapter 1 and meet the requirements for generating high-order harmonics, the necessary theory for laser design is presented. The laser output will need to be amplified in order to have an intensity of $10^{13} W/cm^2$. The method of amplification used in this project is an enhancement cavity, a cavity which is similar in many respects to a laser oscillator, but without a gain medium. The overall design of the source developed for this thesis is shown in Figure 2.1. It consists of a modelocked laser oscillator, an enhancement cavity, and a feedback control system to lock the cavity to the oscillator. The output of the laser is a pulse train and is injected to the enhancement cavity, which enhances the pulse energy due to the high finesse (or quality) of the cavity. In order to obtain the phase coherent amplification, control electronics which lock the oscillator to the enhancement cavity are a necessary component of the setup.

In this chapter, several technical issues related to the design and implementation of the source shown in Figure 2.1 will be discussed. In section 2.1, design considerations to obtain high peak powers from the laser oscillator while limiting the spectral bandwidth are discussed. In section 2.2 the theory behind a pulsed enhancement cavity is covered, including underlying motivation as well as technically relevant issues such as modematching to the enhancement cavity and EUV output coupling schemes. In section 2.3 the technique employed to generate an optical error signal for the feedback control electronics is reviewed.

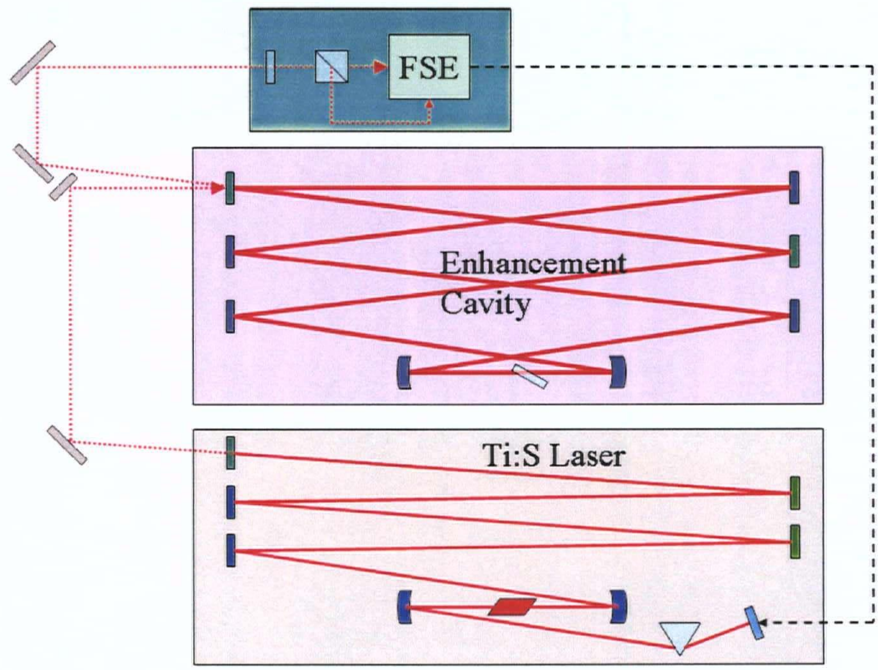

Figure 2.1: The schematic for the source. The Ti:Sapphire laser output (red short dash) feeds into the enhancement cavity (EC) which amplifies the source. A signal is generated from the EC, fed into feedback stabilizing electronics (FSE) which send an electronic signal (black long dash) controlling a mirror in the Ti:Sapph laser. Further details and schematics are given in the relevant sections.

As the end goal is generation of EUV radiation via HHG, the final section 2.4 contains a review of semi-classical theory of HHG.

2.1 The Laser Oscillator

An ideal continuous wave (CW) laser accesses only one resonant frequency mode of the cavity, and thus has a constant intensity and a very narrow linewidth. The peak power of a CW laser is the average power, which typically ranges from a few milliwatts to several watts. In order to have a higher peak power table-top laser oscillator, we use a modelocked laser oscillator. This laser allows for the creation of a pulse train, where the peak power of a pulse is many orders of magnitude higher than the average power.

2.1.1 Gain Medium: the Titanium Sapphire Crystal

The laser source used for the research in this thesis is based on a titanium sapphire (Ti:Sapph) crystal because of several factors which are key to obtaining the high intensities required for the generation of high harmonics. In order to produce its characteristic broad bandwidth from $700 - 1000nm$, the Ti:Sapph crystal is pumped at $532nm$ which is a convenient pump wavelength. The crystal also has a high tolerance for heat and can be pumped at high powers, and has negligible thermal birefringence. Moreover, it has a broad fluorescence spectrum which allows for a wide lasing bandwidth. The broad bandwidth can either be useful for a CW laser which can be tuned over a large bandwidth, or all frequencies can be added in phase so as to create ultrashort femtosecond pulses. The pulse train, which is the output of the modelocked laser, is stable both in frequency and time meaning that the spectrum and duration of each pulse is identical to the one before.

2.1.2 Lasing and Modelocking

For the CW case, only one of the frequencies is amplified within the cavity allowing for a beam of constant intensity. The field inside a CW laser is given as

$$E(z,t) = E_0 e^{i(k_m z - \omega_m t)} + c.c. \tag{2.1}$$

where E_0 is the field strength and *c.c.* is the complex conjugate. The wavevector k and natural frequency ω are denoted by m since it is the m^{th} longitudinal mode that is resonant within the cavity. That is, m is the number of times a given wavelength λ can oscillate within a cavity of length L traveling at speed c, or $\lambda = 2L/m$ for a linear cavity. This implies

$$\begin{aligned} k_m &= \frac{m\pi}{L} \\ \omega_m &= \frac{m\pi c}{L} \end{aligned} \tag{2.2}$$

where $m = 1, 2, 3...$[1]

In the modelocked case, a broad spectrum composed of many ω_m is resonant within the cavity and amplified. Each one of these frequencies (or longitudinal modes) has a very narrow linewidth [7] which make up a small component of the laser output. The field in the modelocked case then becomes the sum of all the individual components. However, in order to account for the phase of the pulse that is generated, there is a carrier envelope phase ϕ_{ce}. The output of a modelocked laser is then

$$E(z,t) = E_0 \sum_{m=n}^{N+n} A_m e^{i(k_m z - \omega_m t + \phi_{ce})} + c.c. \tag{2.3}$$

where the gain medium dictates n, N, and A_m. This is because the gain has a finite bandwidth which begins at some frequency $\nu_n = n\frac{c}{2L}$ and ends at

[1] This argument is valid for a cavity with no dispersive optical elements. For a discussion of cavities with dispersion, see Ref. [8].

$\nu_{N+n} = (N+n)\frac{c}{2L}$, and each spectral component has a relative gain amplitude denoted by A_m.

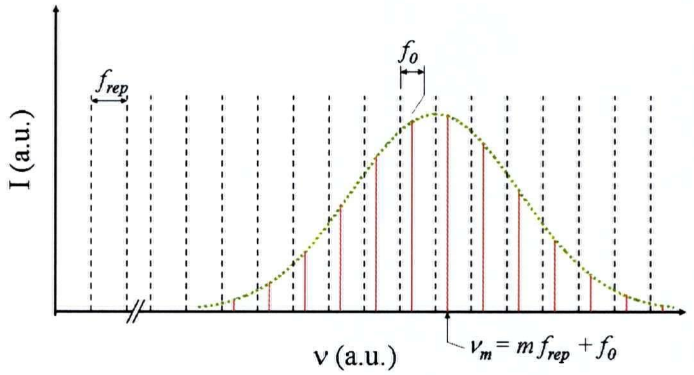

Figure 2.2: The frequency spectrum of a modelocked laser (taken from Ref. [9]). The longitudinal modes ν_m of an empty cavity (black dashed vertical lines) are shifted by an offset frequency f_0 due to the dispersive elements in the cavity. The spectrum of the laser (green dotted curve) is actually the envelope of the frequency comb (red solid vertical lines).

As the output spectrum of a modelocked oscillator is a series of individual modes, it is generally referred to as a frequency comb as can be seen in Figure 2.2. The pulse that is formed within the cavity has a repetition rate that is given as

$$f_{rep} = \frac{c}{2L} \tag{2.4}$$

which is the fundamental mode of the frequency of the laser in the CW case

$$\frac{\omega_1}{2\pi} = \frac{c}{2L}$$

By including a time dependence in the phase in the carrier envelope $\phi_{ce}(t)$, there is a constant shift in the spectrum which is now given as

$$\nu_m = m f_{rep} + f_0 \tag{2.5}$$

The optical frequency of a mode, ν_m, is then some multiple of the repetition rate of the oscillator adjusted by an offset frequency, f_0 [8] (discussed in detail in section 2.1.4).

The number of modes involved in generating the pulse depends on the bandwidth of the pulse, as well as the cavity length. Using $\nu = c/\lambda$ such that frequency bandwidth is related to the wavelength by $\Delta\nu = \frac{c}{\lambda^2}\Delta\lambda$, the number of modes ΔM which make up a pulse of bandwidth $\Delta\lambda$ is

$$\Delta M \approx \frac{2L}{\lambda^2}\Delta\lambda \tag{2.6}$$

for a linear cavity. The consequence of the coherent addition of modes is that as the number of modes increases, the pulse duration decreases (for a given cavity length). This can be seen from finding the full width at half maximum (FWHM) of the pulse in frequency (see Figure 2.2) and time gives the relation

$$\Delta\nu\Delta t = const \tag{2.7}$$

where the constant is dependent on the assumed shape of the pulse (for square pulses $const \approx 0.886$, for gaussian pulses $const = \frac{2}{\pi}ln(2) \approx 0.441$, and for hyperbolic secant squared pulses $const = \left[\frac{\sqrt{2}}{\pi}sech^{-1}(\frac{1}{2})\right]^2 \approx 0.351$). Therefore by combining equations (2.6) and (2.7), for ultrashort (femtosecond) pulse generation there are an enormous number of modes.

To calculate the peak intensity, we need to investigate both the temporal and spatial domains of a series of square pulses with a gaussian spatial profile. The peak power relative to the average power is given as

$$P_{peak} \approx \frac{P_{avg}}{f_{rep}\tau} \tag{2.8}$$

where P_{avg} is the average output power, τ is the pulse duration and f_{rep} is the repetition rate. It becomes apparent that the shorter the pulse and the lower the repetition rate (the longer the cavity, in effect), the higher the peak power.

If we then translate this to intensity, it is found to be [10]

$$I_{peak} = \frac{2P_{peak}}{\pi w_0^2} \tag{2.9}$$

where the factor of 2 is introduced because the spatial profile is assumed gaussian.

To determine how much the output power of a standard Ti:Sapph must be amplified in order to reach the threshold of HHG (typically on the order of $10^{13}W/cm^2$), an example is given. A $100MHz$ oscillator with 1 picosecond ($1ps = 10^{-12}s$) pulse duration and an average output power of $1W$ focused to a spot size of $20\mu m$ has a peak intensity of $\sim 6 \times 10^9 W/cm^2$. Thus, it is necessary that the intensity is increased by 4 orders of magnitude, requiring modifications to the laser oscillator and the use of an amplification scheme.

2.1.3 Limiting the Bandwidth

Since the EUV generated pulses share the characteristics of the fundamental, the narrower the bandwidth of the Ti:Sapph laser output, the narrower the bandwidth of the EUV[2]. Thus, it is required to limit the bandwidth of the Ti:Sapph laser output. As stated in Chapter 1, the goal of the spectral resolution of the EUV is on the order of $E/\Delta E > 5000$, therefore the fundamental must have an approximate bandwidth less than a tenth of a nanometer. From the frequency-time relation of equation (2.7), the pulse duration would then be nearly $10ps$. Although such spectral resolution is the ultimate goal, this narrow bandwidth substantially decreases the peak power (and peak intensity). In order to reach the threshold intensity for these experiments, the initial target pulse duration is on the order of a picosecond.

A method that is useful in limiting the bandwidth of the oscillator is inserting

[2]It is observed in Ref. [11] that the relative bandwidth of the $9^{th} - 15^{th}$ harmonics is broader than the fundamental by a factor of 2.

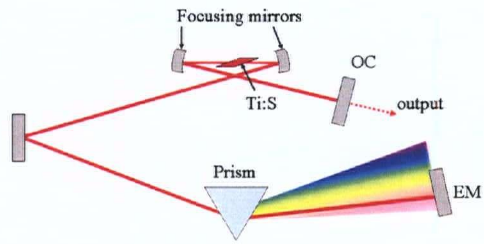

Figure 2.3: Schematic of a bandwidth limited cavity. The prism is used to spatially separate the spectrum, forcing only a fraction of the available bandwidth to be stable within the cavity. EM is the end mirror, OC the output coupler and Ti:S is the Ti:Sapphire crystal.

a single prism into the cavity. As the broad spectrum enters the prism, the beam becomes spatially separated depending on the wavelength. The light propagates the length of the oscillator and the broad bandwidth will become limited as the mirror will only reflect a portion of the spectrum, the part that is resonant inside the cavity (see Figure 2.3). A potential problem with this method would be that there could be a spatial chirp, that is that the central wavelength is spatially (ie tangentially) varying across the profile of the beam. This, however, has not been observed. Although the reasons have not been investigated, one possible explanation is that since the output coupler is flat, the radius of curvature of the beam (as discussed in section 2.1.5) is infinite, meaning that there is a focal point on the face of the output coupler. Therefore, even though the prism causes the beam to be spatially dispersed, the beam is refocused and recombined at the output coupler, canceling the spatial chirp.

By exploiting the spatial dispersion caused by the prism, we are able to limit the supported bandwidth within the cavity. Referring to Figure 2.4 and following from the notation in Ref. [12], it is found that

$$\alpha = \theta_2(\lambda) + \theta_3(\lambda) \tag{2.10}$$

Since the losses due to the prism are to be minimized, the incident beam is at

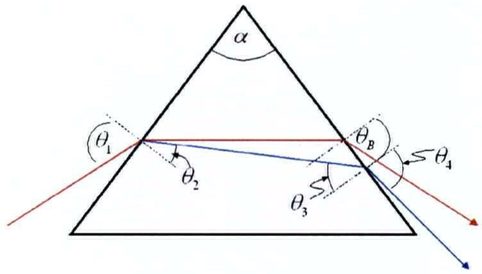

Figure 2.4: The dispersion from a prism. θ_1 is the incident angle, and is set to be the Brewster angle for the central wavelength (here $\lambda_0 = 800nm$) in order to minimize loss. The prism is cut (the peak angle α) such that the output at λ_0 is also at Brewster angle.

Brewster's angle for the central wavelength λ_0. For a well designed (ie symmetrical for the central wavelength) prism, the final resulting angle (θ_4) is also at Brewster's angle. The benefit of the Brewster's angle is that when a prism is inserted into a cavity, it is not an optic that causes much loss. As demonstrated in Figure 2.4, the dispersion results in spatial separation of the frequencies. Using Snell's law to find the resulting angle $\theta_2(\lambda)$,

$$\theta_2(\lambda) = \sin^{-1}\left(\frac{\sin\theta_B(\lambda_0)}{n(\lambda)}\right) \tag{2.11}$$

This then results in $\theta_3 = \alpha - \sin^{-1}\left(\frac{\sin\theta_B(\lambda_0)}{n(\lambda)}\right)$, which means that for the output beam, the final angle is

$$\theta_4(\lambda) = \sin^{-1}\left[n(\lambda)\sin\left(\alpha - \sin^{-1}\left(\frac{\sin\theta_B(\lambda_0)}{n(\lambda)}\right)\right)\right] \tag{2.12}$$

where all the functions of λ have been made explicit, demonstrating the wavelength limiting effects. The dispersion of the prism is calculated by the index of refraction given in Figure 2.5 (a), using the Sellmeier constants found from Ref. [13].

Assuming that this beam reflects off an end mirror at some distance d, the

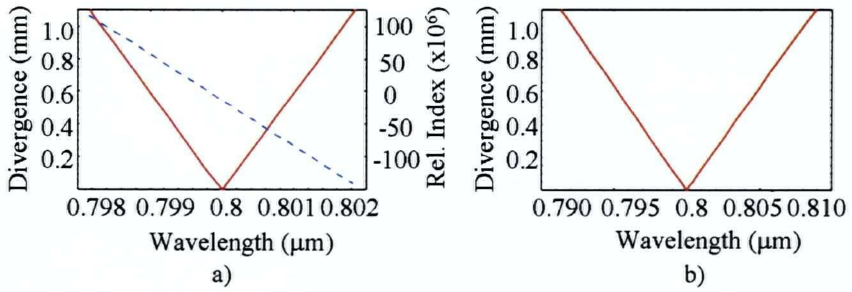

Figure 2.5: The dispersion of the prism limiting the bandwidth. a) The relative index of refraction $n(\lambda) - n(0.8)$ for SF10 (blue dash) (where $n(0.8) = 1.71124$) and the divergence of the beam for a cavity length of $d = 6m$. The spread of the beam size is due to the dispersion of the prism. The calculated waist of the beam is $w = 0.6mm$, so the supported bandwidth is predicted to be $\Delta\lambda \approx 2nm$. b) For a low-dispersion material such as CaF_2, the bandwidth is predicted to be much greater.

size of the waist of the beam will be given as

$$\Delta w_0 = |d \tan(\theta_4(\lambda) - \theta_B(\lambda_0))| \tag{2.13}$$

where the limitation of this approximation comes from the fact that an infinitely small initial waist has been assumed at the front interface of the prism. The calculation for cavity stability is done in section 2.1.5, a calculation which gives the size of a gaussian beam throughout the cavity given a certain mirror configuration. The prism has a flat interface, and so has minimal effect on the cavity stability and waist at the output coupler and end mirror. The bandwidth of the laser comes from the wavelengths that are not spatially dispersed far from λ_0 (where 'far' is defined here as being greater than the beam waist at the output coupler or end mirror). This method gives a good first order calculation for the bandwidth of the oscillator.

In equation (2.13), the factors which affect the bandwidth are the cavity length (and beam waist), the central wavelength, and the index of refraction of the prism. Since the cavity length and beam waist are determined by the stable cavity parameters (described in section 2.1.5), this is not a parameter that is easily modified by a prism (due to its flat interfaces). The main bandwidth-limiting parameter that is available is the type of glass that is inserted into the cavity as demonstrated in Figure 2.5.

If the spectral resolution is still insufficient, the bandwidth can be further narrowed by using additional prisms. By orienting the two prisms the same direction, the amount of spatial dispersion with be increased (see Figure 2.7(b)).

Although other methods could be used for limiting the bandwidth, a prism is beneficial for several reasons. First, by slightly adjusting the input angle it is possible to select the central wavelength of the oscillator over most of the supported bandwidth of the crystal (about 200nm). This is useful since the reflectivity of the mirrors in the enhancement cavity is dependent on the wavelength. Thus, tuning the central wavelength so that the enhancement cavity has the highest possible finesse (proportional to the reflectivity of the mirrors) allows for a higher enhancement factor (to be discussed later). Also, prisms are often used to compensate for dispersion (to be discussed in section 2.1.4). Since prisms are often already used in cavities for dispersion compensation, no additional optical elements are required if they are also used to control the bandwidth.

2.1.4 Dispersion Compensation

In order for a pulse to be stable and self-consistent within a cavity, each frequency component of the pulse must have the same repetition rate (or period) within the cavity. This is implied by equation (2.5) since there is an equal spacing between each frequency component. To understand how this can occur, we need to investigate the relation between the wavevector k and the frequency ω. The velocity of a single frequency component ω in an optic with index of refraction n is given by the phase velocity

$$v_p = \frac{\omega}{k} = \frac{c}{n(\omega)} \tag{2.14}$$

which can be rearranged to show that $k(\omega) = \omega\frac{c}{n(\omega)}$. It is possible to expand the wavevector about a central frequency ω_0, relating each term to some physical quantity.

$$k(\omega) = k(\omega_0) + (\omega - \omega_0)\frac{\partial k}{\partial \omega} + \frac{(\omega-\omega_0)^2}{2}\frac{\partial^2 k}{\partial \omega^2} + \frac{(\omega-\omega_0)^3}{6}\frac{\partial^3 k}{\partial \omega^3} + \cdots \tag{2.15}$$

The zeroth term in the series is simply the wavevector at the central frequency, while the first term is related to the group velocity

$$v_g = \left(\frac{\partial k(\omega)}{\partial \omega}\right)^{-1} \tag{2.16}$$

The second term relates the dependence of the group velocity on the frequency, and so the second term is called the group velocity dispersion (GVD) and is typically represented in units of fs^2/mm.

An element with a dispersion of zero implies that all the frequency components of the pulse have the same group velocity, and thus the pulse will keep its shape as it propagates through the element. In a dispersionless cavity, the group velocity is independent of the frequency so the round trip time for each frequency component is also independent of frequency. Since a pulse makes many round trips within a cavity, the dispersion within the Ti:Sapph oscillator must be carefully tuned to allow for the creation of a stable pulse train.

If the dispersion of an optical element is non-zero, then some frequency components will lead while others lag; this leads to a chirp. A chirped pulse has some temporal dependence on the constituent frequencies implying that the pulse duration will not relate to the bandwidth of the pulse as dictated in equation (2.7). Using the relation that the time required for a frequency component to propagate through an optical element of thickness L is given by $\tau = L/v_g$, then the change in the pulse duration is found to be [10]

$$\begin{aligned} \Delta\tau &\approx L\Delta\omega \left| \frac{\partial^2 k}{\partial \omega^2} \right| \\ &= \frac{\Delta\lambda L}{c} \left| \frac{\partial^2 n}{\partial \lambda^2} \right| \end{aligned} \tag{2.17}$$

where the bandwidth of the pulse is $\Delta\omega$ or $\Delta\lambda$ and the index of refraction is n. Because of the increase in pulse duration, the peak power of a chirped pulse will be lower than that of a transform-limited pulse. Thus, for this experiment a chirped pulse is not desired.

There is an additional effect known as self-phase modulation (SPM) that must also be compensated. This is a nonlinear effect due to the high peak intensity of the pulse. The high peak intensity of the pulse can change the index of refraction of an optical material, which effectively adds more normal dispersion.

Often group delay dispersion (GDD) is used instead of GVD as a convenient measure when the propagation distance through an optical element is known, and can be found by using the relation $\phi(\omega) = Lk(\omega)$ where L is the distance of propagation within the optic. In discussing the amount of dispersion within the cavity, it is the net GDD which will be discussed in this thesis as some optics have negligible propagation distance, but have a resulting GDD (such as chirped mirrors). The third order term (third order dispersion, or TOD) has become important in the case of ultrashort pulse generation, but in the current discussion of a few nanometers of bandwidth, it is of little concern [14].

The causes for the dispersion in the cavity come from the optical elements and the Ti:Sapphire crystal itself. In the visible and near infrared part of the spectrum, most material causes normal dispersion (a positive value when discussing the index of refraction in terms of wavelength), while anomalous disper-

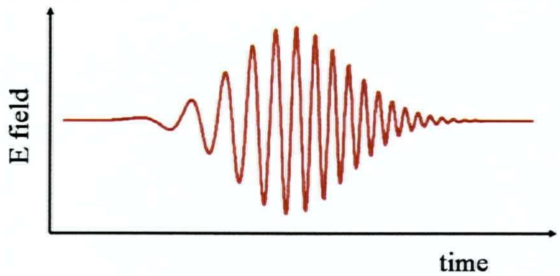

Figure 2.6: An upchirped pulse

sion carries the opposite sign. The main source of positive dispersion within the laser cavity is the crystal. In order to introduce anomalous dispersion into the cavity, two common methods have been developed. Special mirrors which have a series of carefully designed dielectric coatings allow for different penetration depths depending on the wavelength, and thus can compensate for the dispersion by adjusting the optical path length of different wavelengths in the cavity. Although there can be an arbitrary amount of these chirped mirrors in a cavity, the amount that they compensate is fixed. To finely adjust any residual dispersion, a prism (pair) is inserted into the laser cavity. By mounting the prism on a translation stage, it is possible to adjust the amount of glass through which the beam passes. This allows the user to finely tune the amount of dispersion within the cavity, a necessary requirement in order to have a stable, passively modelocked oscillator.

Material	n(800nm)	v_g/c	GDD (fs^2)
Sapphire (n_o)	1.76	0.561	133
CaF_2	1.43	0.695	27.9/mm
SF10	1.71	0.571	159/mm
M_i	–	–	-70

Table 2.1: Table of materials used in the oscillator and their group velocity and delay dispersion values; c is the speed of light; M_i represents one of the 4 mirrors that are dispersion compensated. Numbers are for single pass through the optic element.

The repetition rate of the pulse is determined by the group velocity of the pulse, v_g, while each frequency component travels at the phase velocity v_p. The offset frequency, f_0, is a consequence of the difference in phase and group velocities [8]

$$f_0 = \frac{\omega_c v_g}{2\pi}\left(\frac{1}{v_g} - \frac{1}{v_p}\right) \tag{2.18}$$

where ω_c is the carrier angular frequency. The offset frequency causes a constant shift in the entire spectrum of the output of a modelocked laser.

To conclude the section on dispersion, several practical matters arising are considered. The index of refraction is usually given in terms of the wavelength λ by the Sellmeier equation. This is an empirical equation which has the form

$$n^2(\lambda) = 1 + \frac{B_1\lambda^2}{\lambda^2 - C_1} + \frac{B_2\lambda^2}{\lambda^2 - C_2} + \frac{B_3\lambda^2}{\lambda^2 - C_3} \tag{2.19}$$

where the constants B_i and C_i are experimentally determined and tabulated [13]. The corresponding group velocity and GVD become

$$\frac{1}{v_g} = \frac{1}{c}\left[n(\lambda) - \lambda\frac{\partial n(\lambda)}{\partial \lambda}\right] \tag{2.20}$$

$$GVD(\lambda) = \frac{\lambda^3}{2\pi c^2}\frac{\partial^2 n(\lambda)}{\partial \lambda^2} \tag{2.21}$$

The GDD from light propagating through a pair of prisms which are oriented as Figure 2.7(a) can also be obtained in closed form. Although the material will have normal dispersion, the geometry dictates that the setup can provide anomalous dispersion, thus providing a means to tune the net cavity dispersion through zero. The GDD for the prism pair is given by Ref. [14]

$$GDD(\lambda) = -4L_{sep}\frac{\lambda_0^3}{2\pi c^2}\left(\frac{\partial n}{\partial \lambda}\right)^2 + L_{prism}\frac{\lambda_0^3}{2\pi c^2}\frac{\partial^2 n}{\partial \lambda^2} \tag{2.22}$$

and is very useful in cases supporting a broad bandwidth.

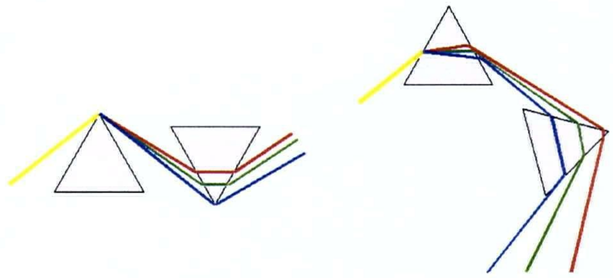

Figure 2.7: Prism pairs used for a) dispersion compensation for maximum bandwidth (see equation (2.22)) and b) extra spatial dispersion to minimize bandwidth.

2.1.5 Laser Cavity Extension via Unity Transform

The narrow spectrum limits the number of modes contributing to the laser field, which means that the peak output power from the oscillator must be regained by some other means. As presented in equation (2.8) and the surrounding discussion, the longer the cavity, the higher the peak power [15]. However, the effect of a longer cavity on the laser operation must be well understood since modelocking and output power can be compromised.

Ray Optics and the Ray Transfer Matrix

If we define a ray of light by its position r from the optic axis z and its slope as $r' = \frac{dr}{dz}$ (see Figure 2.8), then the resulting ray through an optical element can be determined with a matrix [16]. This matrix is a mathematical description for the direction of propagation for ray optics, and it represents the effect the optic has on r and r'. Each optical element has its own matrix representation.

The matrix is obtained by the following method. A ray of initial position r_i and direction of propagation relative to the z axis $\sin(\theta_i)$ encounters an optic,

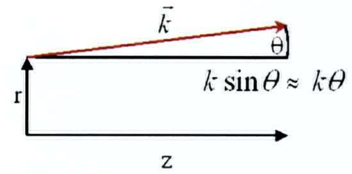

Figure 2.8: A ray propagating in direction $\vec{k}$ through space. The slope of the beam relative to the z axis is typically small such that $\tan\theta \approx \sin\theta \approx \theta$.

resulting in the position and direction

$$\begin{aligned} r_f &= Ar_i + B\sin(\theta_i) \\ \sin(\theta_f) &= Cr_i + D\sin(\theta_i) \end{aligned} \tag{2.23}$$

These two equations can then be generalised to a matrix, as represented by

$$\begin{pmatrix} r_f \\ \sin(\theta_f) \end{pmatrix} = \begin{pmatrix} A & B \\ C & D \end{pmatrix} \begin{pmatrix} r_i \\ \sin(\theta_i) \end{pmatrix} \tag{2.24}$$

The matrix acting on the ray is the ray transfer matrix.

The Paraxial Approximation and Gaussian Beams

The electric field must be a solution to the vector wave equation

$$(\nabla^2 + k^2)\vec{E}(x, y, z) = 0 \tag{2.25}$$

where ∇^2 is the Laplacian. On the condition that we have a well collimated laser beam (as is usually the case for stable lasers) that is propagating in the z direction, the field can be separated as

$$\vec{E}(\vec{r}) = \vec{E}_0(\vec{r})e^{ikz} \tag{2.26}$$

It is implied that the dependence of $E_0(\vec{r})$ on z is much less than on x, y over the distance of a few wavelengths. Quantitatively, this becomes

$$\left|\frac{\partial^2 E_0(\vec{r})}{\partial z^2}\right| \ll k^2 \left|E_0(\vec{r})\right| \tag{2.27}$$

The wave equation can then be reduced to the paraxial wave equation, which is found to be [10]

$$\left(\frac{\partial^2}{\partial x^2} + \frac{\partial^2}{\partial y^2} + 2ik\frac{\partial}{\partial z}\right)\vec{E}_0(\vec{r}) = 0 \tag{2.28}$$

which has a solution

$$\vec{E}_0(\vec{r}) = \vec{A}e^{ikz}\frac{w(z)}{w_0}e^{ik(x^2+y^2)/2R(z)}e^{-i\phi(z)}e^{-(x^2+y^2)/w^2(z)} \tag{2.29}$$

where $\vec{A}$ is some amplitude constant in the direction of polarization and w_0 is the minimum beam waist. This solution has a gaussian envelope, and so the resulting field from a laser with this profile is referred to as a gaussian beam. The parameters are defined in Table (2.2).

$z_0 = \pi w_0^2/\lambda$	Rayleigh Range
$w(z) = w_0\sqrt{1 + z^2/z_0^2}$	beam waist
$R(z) = z\left(1 + z_0^2/z^2\right)$	radius of curvature
$\theta = \lambda/\pi w_0$	divergence angle
$\phi(z) = \tan^{-1}(z/z_0)$	Guoy phase

Table 2.2: Gaussian beam parameters taken from [10]

The exponent in equation (2.29) can be combined to a single term $q(z)$, which is defined as

$$\frac{1}{q(z)} \equiv \frac{1}{R(z)} + \frac{i\lambda}{\pi w^2(z)} \tag{2.30}$$

The $q(z)$ parameter uniquely determines the properties of a gaussian beam. This parameter can be modified as it passes through optical elements, which are mathematically described by some coefficients A, B, C, and D[3]. A new q_f is related to the initial q_i by

$$q_f = \frac{Aq_i + B}{Cq_i + D} \tag{2.31}$$

For any given cavity, the stability criterion is that the spot size at a given location within the cavity is not diverging, and so the beam waist and radius of curvature must be identical after many round trips. This means that after traveling one cavity length ($2L_0$ for a linear cavity) we get $q(2L_0) = q(0)$. Combining this with equation (2.31), it is found that

$$\frac{1}{q} = \frac{D - A}{2B} \pm \frac{\sqrt{(A-D)^2 + 4BC}}{2B} \tag{2.32}$$

This q then dictates the stability conditions based on the geometry of a cavity given by the ABCD coefficients.

2.1.6 The ABCD Matrix

The results from ray optics can be used in gaussian optics since equation (2.31) can be rewritten as

$$\begin{pmatrix} q_f \\ 1 \end{pmatrix} = \begin{pmatrix} A & B \\ C & D \end{pmatrix} \begin{pmatrix} q_i \\ 1 \end{pmatrix} \tag{2.33}$$

The matrix acting on the q parameter is also the ray transfer matrix, however is generally referred to as the ABCD matrix when discussing gaussian beams [16]. It is convenient to use the ABCD matrix since the matrix elements can easy be calculated (either from ray optics or gaussian optics), and can easily be extended to represent many optical elements, and their combinations. The consequence of a gaussian beam propagating through multiple optical elements becomes the product of these ABCD matrices, cascaded in reverse order of

[3]These coefficients are unique to each optical element, and are given in references [10, 17]. They are also the matrix coefficients in the ray transfer matrix as discussed in section 2.1.5.

propagation. That is, the ABCD matrix of an entire cavity with N optical elements is given by

$$\begin{pmatrix} A & B \\ C & D \end{pmatrix} = \mathbf{M_N M_{N-1} \cdots M_2 M_1} \tag{2.34}$$

where each M_i is an ABCD matrix determined by the optical element it represents[4]. A property of the ABCD matrix is that its determinant is unity. This allows equation (2.32) to be rewritten as

$$\frac{1}{q} = \frac{D-A}{2B} \pm \frac{\sqrt{(A+D)^2-4}}{2B} \tag{2.35}$$

This is similar to equation (2.30), the real part is associated with the first term, while the imaginary is with the second term. Since it is required to have some finite waist w_0, then the argument under the square root must be negative, or $(A+D)^2-4) < 0$. This then leads to the stability condition of a cavity, which is

$$\frac{1}{2}|A+D| < 1 \tag{2.36}$$

where A and D depend on the cavity geometry.

2.1.7 Cavity Extension

As is mentioned in section 2.1.2, the intensity of the output intensity of a standard ps, $100MHz$ Ti:Sapph oscillator is 4 orders of magnitude below the threshold required for HHG. Although the ideal amplification of an enhancement cavity could create the necessary intensity, practical considerations limit the enhancement factor to several hundred [18–20]. Thus, in order to maximize the photon energy stored within the enhancement cavity, our Ti:Sapph laser is a modifica-

[4]The ABCD matrix is also used to guide the laser output. Collimating the beam is useful in this project since the output of the laser is injected into an enhancement cavity. This is discussed further in section 3.2

tion from the standard design. The relation of average to peak power is given in equation (2.8), which implies that by extending the laser cavity it is possible to have a higher peak power.

The original design of our Ti:Sapphire oscillator was an octave spanning laser for high precision metrology [21], and so the modematching and modelocking parameters are already well understood and optimized for efficient, stable output. Thus, when this cavity is designed to be extended from a repetition rate of $82MHz$ down to $25MHz$, it is desired to minimize the changes to the cavity. Specifically, the radius of curvature and waist of the beam inside the crystal and at the output coupler for the shorter case are identical to those in the longer case.

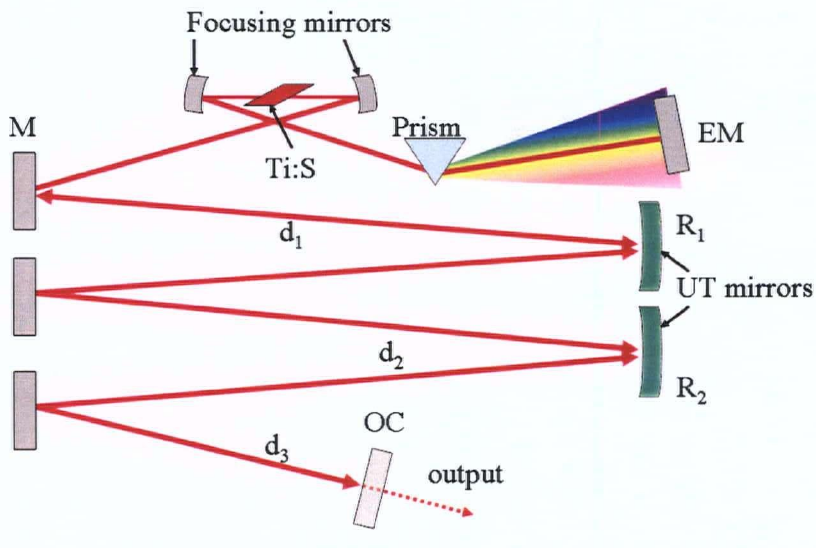

Figure 2.9: The extended (25MHz) cavity schematics. The two unity transform (UT) mirrors have a long focal length such that the q parameter is the same at the end mirror (EM) and output coupler (OC) as in Figure 2.3. Instead of the OC being at position M, it is replaced by a series of mirrors with radius of curvatures R_1 and R_2, and propagates a total distance $d_1 + d_2 + d_3$. d_1 is the distance from M to the first UT mirror, d_2 the separation of the UT mirrors, and d_3 is the distance from the UT mirror to the OC.

The short cavity geometry gives the waist at the output coupler w_{oc}. For the short cavity in Figure 2.3, the q parameter at the output coupler is purely imaginary as a flat output coupler dictates that the radius of curvature is infinite. The beam waist at the output coupler for the short cavity w_{oc} is the same as for the long cavity case by construction, and so $q_{oc}(long) = q_{oc}(short)$. This allows the use of equation (2.32), and noting that the beam profile is flat at the output coupler, then $A = D$. Putting this together, the beam is defined as

$$\frac{i\lambda}{\pi w_{oc}^2} = \frac{\sqrt{(A+1)(A-1)}}{B} \tag{2.37}$$

where the coefficients A and B are found to be

$$\begin{aligned} A &= 1 - \frac{2d_1}{R_1} - \frac{2(d_1 + d_2(1 - \frac{2d_1}{R_1}))}{R_2} \\ B &= d_1 + d_2(1 - \frac{2d_1}{R_1}) + d_3\left(1 - \frac{2d_1}{R_1} - \frac{2(d_1 + d_2(1 - \frac{2d_1}{R_1}))}{R_2}\right) \end{aligned} \tag{2.38}$$

where the d_i's and R_i's are defined in Figure 2.9. This is now a problem with 5 parameters, but this can be simplified with a few practical considerations (see Appendix C.1). The parameters are now chosen dependent on the wavelength of the oscillator and the waist at the output coupler for the shorter cavity.

2.2 Enhancement Cavity

The use of an enhancement cavity (EC) as the amplifier in this project is chosen because of the high photon flux which can be attained from a high repetition rate. The EC uses high reflectivity mirrors to store light for an extended period of time. As an applied field from a laser in injected into the cavity, the power can build up by several orders of magnitude which is due to the coherent addition of the field from many round trips. This system does not use a gain medium, eliminating concerns about noise and spectral broadening. However, the EC has many of the same issues as the oscillator with regards to cavity stability, modematching, and dispersion. Due to the high reflectivity of the mirrors inside the EC, many of these factors are more pronounced and are more sensitive as compared to laser cavities. For example, the transmission of the output coupler for the laser oscillator is 10% while for the input coupler of the EC, the transmission can be as low as 0.1%. This translates to a factor of 100 times increase in photon lifetime in the EC than in the laser oscillator. Therefore, the pulse has many roundtrips within the EC, and so is very sensitive to the dispersion of optical elements. Thus any errors in alignment or dispersion will become greatly amplified and so proper setup of an EC is not trivial.

2.2.1 Intensity Enhancement

Enhancement cavities have existed almost as long as lasers themselves [22]. The use of an EC to amplify a CW laser to reach the threshold for second or third harmonic generation (SHG or THG) is beneficial because the harmonic is then also a clean, narrow linewidth signal. For nonlinear phenomena such as SHG, enhancement cavities have been used for CW lasers where the output from an oscillator is not intense enough in order to observe these nonlinear effects. The original case of a single-mode ring cavity will be the starting point for the discussion of enhancement cavities as it is a simpler case. The single mode case can then be extended to model a pulse resonating in the EC.

Single Mode Ring Cavity

For CW operation, the input field E_0 is incident on the input coupler with a reflectance $r_{ic} = \sqrt{R_{ic}}$ and transmission coefficient $T_{ic} = 1 - R_{ic}$. For a cavity with no output coupler, there will be some given loss $L = 1 - l^2$, where $l \sim r^N$ with N is the number of mirrors in the cavity. This assumes that all loss is at the mirrors and they are all equal. In this project, there is a Brewster plate which will also cause some loss. In any case, the loss l will account for any

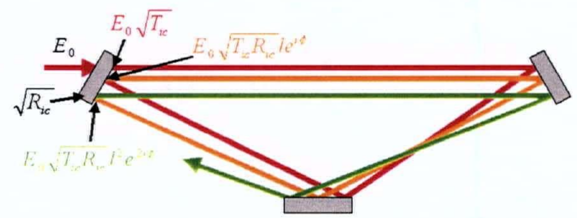

Figure 2.10: The electric field inside a ring cavity. The input electric field E_0 is incident on the input coupler with reflection coefficient $R_{ic} = r_{ic}^2$. After one round trip, it has a phase $\phi = kd$ where k is the wavevector and d is the cavity length. Provided there is an applied field, the constructive interference causes a large enhancement without a gain medium in the cavity.

scattering/absorption that may occur. The field after traveling through the cavity of length d has a phase $\phi = kd$. The field then at the input coupler due to a series of round trips becomes

$$E_{cav} = E_0\sqrt{T_{ic}}\,(1 + lr_{ic}e^{i\phi} + (lr_{ic}e^{i\phi})^2 + (lr_{ic}e^{i\phi})^3 + \cdots) \tag{2.39}$$

which is a geometric series and converges to

$$E_{cav} = \frac{E_0\sqrt{T_{ic}}}{1 - lr_{ic}e^{i\phi}} \tag{2.40}$$

Since it is the intensity that is crucial for this experiment, the intracavity intensity becomes

$$I_{cav} = \frac{I_0 T_{ic}}{(1 - lr_{ic})^2 + 4lr_{ic}\sin^2(\frac{\phi}{2})} \tag{2.41}$$

A useful measurement of the cavity is the finesse, which is given by

$$\mathcal{F} = \frac{\pi\sqrt{lr_{ic}}}{1 - lr_{ic}} \tag{2.42}$$

The finesse determines the FWHM of the linewidth of the modes inside a cavity by

$$\Delta\nu = \frac{\nu_{FSR}}{2\pi}\sin^{-1}\left(\frac{2\pi}{\mathcal{F}}\right) \approx \nu_{FSR}/\mathcal{F} \tag{2.43}$$

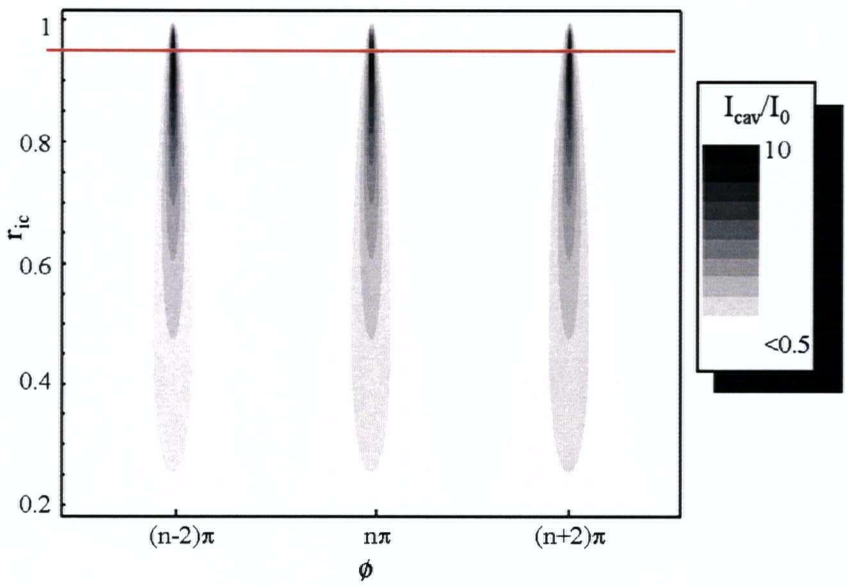

Figure 2.11: Contour plot of the relative intracavity intensity I_{cav}/I_0 as a function of both the input coupler reflectance $r_{ic} = \sqrt{R_{ic}}$ and phase ϕ for a ring cavity. The intracavity intensity is maximized when R_{ic} equals the losses of the cavity $L = 1 - l^2$ and $\phi = 2n\pi$ where n is an integer. When $R_{ic} = 1 - L$, the cavity is said to be impedance matched, and is shown by the line at $r_{ic} \approx 0.95$ ($T_{ic} = 10\%$). An undercoupled cavity where $r_{ic} > l$ quickly loses the enhancement efficiency. Notice that the lower r_{ic} allows for a greater range in ϕ for the same I_{cav}/I_0.

The finesse is also a useful tool since the losses inside the cavity determine the photon lifetime τ_p. This is related to the finesse by

$$\tau_p = \frac{\mathcal{F}}{2\pi\nu_{FSR}} \tag{2.44}$$

The finesse of the cavity is then a very useful tool when predicting the enhancement characteristics of the cavity. It will be used many times in discussing the features of the EC.

From Figure 2.12, the enhancement factor is dependent on the roundtrip phase of the field inside the cavity, ϕ. Since the intensity peaks every $2m\pi$ where m is some integer, the length of the cavity must be $d = m\lambda$. This means

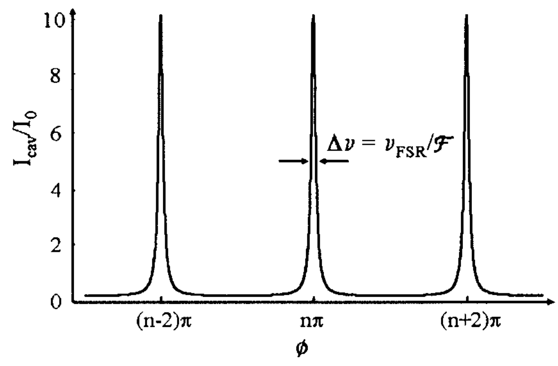

Figure 2.12: A cross-sectional slice of Figure 2.11 at $r_{ic} = 0.95$, which gives a peak relative intensity $I_{cav}/I_0 = 10$. The full width half maximum (FWHM) of each mode is the ratio of the frequency to the finesse, $\mathcal{F}$, of the cavity.

that for maximum amplification, the EC length must be an integer multiple of the wavelength of the fundamental beam. This is the motivation for a locking mechanism that can control the cavity lengths (discussed in section 2.3). Assuming that the EC length is locked, for a given amount of loss in the cavity (via frequency conversion, scattering at the mirrors, etc) the optimal enhancement occurs when the reflection coefficient of the input coupler can match this loss (this situation is referred to as impedance matched). In this case the typical enhancement possible is

$$I_{cav} \approx \frac{I_0}{1-R} \approx I_0 \frac{\mathcal{F}}{\pi} \tag{2.45}$$

for $1-R \ll 1$. Therefore, a high finesse cavity $\mathcal{F} \sim 10^3$ can have an enhancement of > 300. So in order to attain high intensities, we are motivated to construct an EC with high finesse.

Multimode Transfer Function

The difference in the output spectrum of CW and modelocked laser operation is the number of modes which must be considered. In the CW case, only a single frequency ω is resonant within the EC, which means that the total length of the

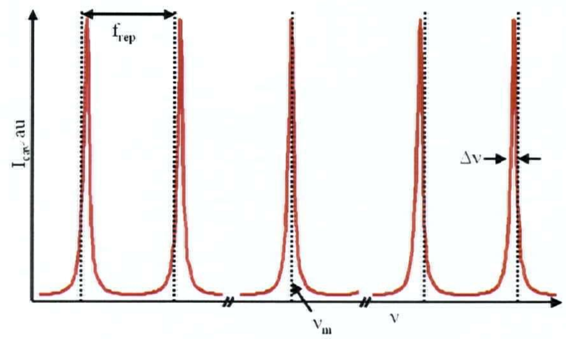

Figure 2.13: The modes of a reference cavity (the EC) (red curve) and the modes of the frequency comb (black dash) for the spectrum. Although the centre mode of the comb is set to a mode of the EC, due to cavity mismatch this is not true for all modes. In order for all modes to be aligned, both f_{rep} and f_0 must be controlled. Although a higher finesse gives a higher intracavity intensity as seen in equation (2.45), this limits the tolerance of the mismatch of the EC to the laser modes, thus limiting enhancement.

enhancement cavity d must satisfy $\frac{\omega d}{c} = 2m\pi$, or

$$\frac{\omega}{2\pi} = \frac{cm}{d} \tag{2.46}$$

where m is an integer. This lack of constraint on d allows for an enhancement cavity to be any size, so long as it is an integer multiple of the wavelength of light it is amplifying.

The CW case can be extended to the modelocked case, however now the number of modes that the EC must support can be enormous ($10^4 - 10^5$). In the modelocked case, each frequency component of the input field must be matched to a respective mode of the EC in order to attain the ideal enhancement. Recall that the modes of a modelocked oscillator are from equation (2.5)

$$\nu_m = mf_{rep} + f_0$$

The difference of the CW and modelocked cases can be seen comparing Figures 2.12 and 2.13. In the ideal multimode case all of the modes are aligned and we have the maximum attainable intracavity power. The comb spacing of the incoming field is set by f_{rep} for the entire spectrum. In order for the spacing of the modes in the EC to match f_{rep}, the length of the EC must be matched to that of the modelocked laser.

As mentioned, the constant f_{rep} in the spectrum implies that the net dispersion of the laser oscillator is zero. However, the dispersion (as well as higher order terms) in the EC is not necessarily zero since optical elements that can finely tune dispersion (such as prisms, etc) cannot be used since they cause too much loss. The presence of dispersion in the EC will cause an unequal spacing of the modes, limiting the bandwidth supported by the EC, and will cause the pulse duration to increase equivalent to the effect seen in equation (2.17). An estimate of the net effect that GDD has on the pulse duration can be seen by combining equations (2.17) and (2.7). The relative amount that an initially transform-limited pulse spreads per pass (pp) in the cavity is

$$\frac{\Delta\tau_{pp}}{\tau} = |GDD| \times \frac{\pi^2 c^2 (\Delta\lambda)^2}{ln(2)\lambda^4} \tag{2.47}$$

which demonstrates the sensitivity of the relative pulse duration to the pulse bandwidth, $\Delta\lambda$. Therefore, within the photon lifetime of a picosecond pulse in an EC of finesse ~ 600, as long as the net GDD is less than $20fs^2$ the relative pulse duration changes by less than 1%.

Additionally, as shown in equation (2.18) there is an offset frequency which comes from the differences in phase and group velocities within the laser cavity. The EC will also have a difference in v_p and v_g due to optical elements (e.g. a Brewster plate), and so it too has its own offset frequency f_0^{EC}. Therefore, even when the repetition rates of the oscillator and EC are equal, the comb lines of the incident field will not align with the modes of the EC because of the difference in f_0 and f_0^{EC}.

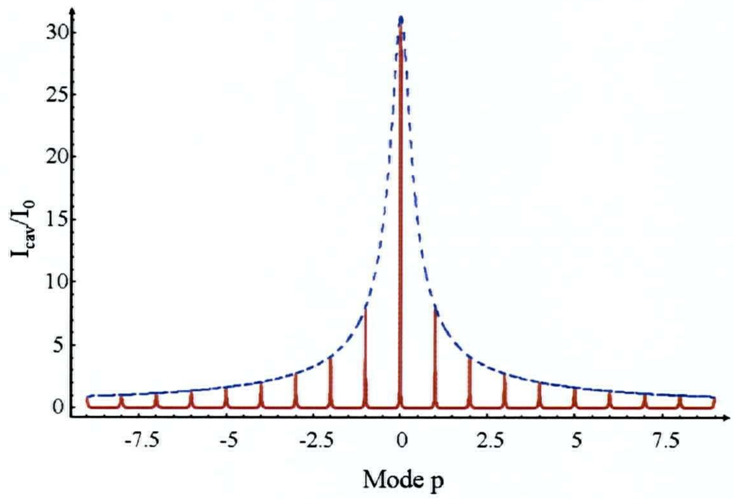

Figure 2.14: Theoretical plot of the enhancement factor as a function of the cavity length mismatch inside the EC. The parameters for the EC are a finesse of 100, a central wavelength $\lambda = 800nm$ and a bandwidth of $\Delta\lambda = 30nm$. Because of the bandwidth of the pulse, there is a Lorentzian lineshape (blue dash) which modifies the modes (solid red). For a single linewidth CW laser the intensity is equal for all modes (see Figure 2.12). The higher finesse and broader bandwidth narrow the width of the Lorentzian envelope, making the locking to the central mode more crucial to reach high intensities. Also note that for larger $|p|$, the width of the mode increases. See reference [23] for comparison.

Now that the consequences of dealing with tens of thousands of modes when using an enhancement cavity have been addressed, we can quantify the effects they have on the enhancement factor. Taking into account the misalignment of the incident field comb lines and the EC modes, the relative intracavity power is given by [23]

$$A(p) \propto \frac{1}{\sqrt{1 + p^2 \left(\frac{\Delta\lambda\mathcal{F}}{\lambda_0}\right)^2}} \tag{2.48}$$

where $\mathcal{F}$ is the finesse of the cavity, $\Delta\lambda$ is the laser bandwidth, and

$$p \propto \frac{f_{rep} - f_{rep}^{EC}}{f_{rep}} + \frac{\delta}{2\pi} \tag{2.49}$$

represents the measure of alignment of the comb and mode spacing. f_{rep}^{EC} is the repetition rate of the enhancement cavity, and $\delta = 2\pi(f_0 - f_0^{EC})/f_{rep}$.

Since the maximum attainable intracavity power is dependent on the finesse in equation (2.45), then for $p \neq 0$ the effective finesse of the cavity is reduced. Therefore, combining equations (2.41) and (2.48), the relative intracavity power N in a multimode enhancement cavity is given by

$$N = \frac{\left(\frac{2\mathcal{F}_{eff}(p)}{\pi}\right)^2 T_{ic}/4}{1 + \left(\frac{2\mathcal{F}_{eff}(p)}{\pi}\right)^2 \sin^2(p\pi)} \tag{2.50}$$

where the effective finesse is given as

$$\left(\frac{2\mathcal{F}_{eff}(p)}{\pi}\right)^2 = \frac{\left(\frac{2\mathcal{F}}{\pi}\right)^2}{\sqrt{1 + p^2\left(\frac{\Delta\lambda\mathcal{F}}{\lambda_0}\right)^2}} \tag{2.51}$$

Two important consequences arise from these equations. First, as the finesse of the EC is now dependent on the mode p, this implies that the linewidth of the enhanced modes will also be affected by the cavity length mismatch. As $|p|$ increases, the finesse of the cavity decreases, which effectively increases the amount of loss in the cavity according to equation (2.42). The linewidth is important when considering the locking mechanism used as described in section 2.3. Second, the differences in the offset frequencies of the comb modes and the EC cause a shift within this envelope. Therefore to obtain the maximum enhancement possible, $\delta \propto f_0 - f_0^{EC}$ must be also controlled.

As δ causes a shift of the modes within the envelope function of equation (2.48), the intracavity power is decreased. By drifting an amount π, then the EC has effectively shifted by one cavity mode and the modes have returned to their original position. Therefore, we need only consider the effects of δ drifting by an amount $\pi/2$ because any further, and we can simply redefine the case for $p = 0$. Using this argument, we can quantify when the importance of the envelope function limits the intracavity power.

For a given central wavelength λ, the value of $\Delta\lambda\mathcal{F}$ dictates the shape of the envelope in Figure 2.14. The FWHM of this function is

$$\Delta p = \frac{2\sqrt{3}\lambda}{\Delta\lambda\mathcal{F}} \tag{2.52}$$

and the bandwidth of the field and the finesse of the cavity are parameters which can be controlled. So then in order to have at least one-half of the maximum attainable intracavity power, the constraint becomes

$$\Delta\lambda\mathcal{F} \leq 2\sqrt{3}\lambda \tag{2.53}$$

Therefore, as long as equation (2.53) is satisfied, then as δ drifts an amount $\pm\pi/2$ the intracavity power will be at least one-half the maximum attainable.[5] If, however, this is not satisfied, then the offset frequency must be controllable.

Since the EC has no tunable elements to adjust f_0^{EC}, the offset frequency of the laser f_0 must be tunable. This can be achieved in the laser cavity by adjusting the insertion of the prism in the beam path [24]. Although the dispersion of the cavity will remain zero, the addition of material in the beam path will change the phase and group velocities, thereby adjusting f_0. Since this changes both the phase and group velocities, it adjusts not only the offset frequency of the laser, but also its repetition rate. Therefore the length of the laser will need to be simultaneously adjusted in order to remain at the fringe $p = 0$.

Another parameter that is adjustable is the power of the pump incident on the Ti:Sapph laser. The nonlinear index of refraction is given as $n_{NL} = n + n_2 I$ where n is the (linear) index of refraction, n_2 is the second order refractive index, and I is the intensity of the applied field. Now in a high intensity case, the index of refraction in the Ti:Sapph crystal depends on the (peak pulse)

[5] The requirement that at least half of the power is achieved is arbitrary, and in fact a system in which the power drifts by this much will be difficult to use in an experiment. To avoid the effect of the drift of the offset frequency on the maximum intracavity power, a satisfactory requirement is $\Delta\lambda\mathcal{F} < \lambda$.

intensity which can be tuned by the pump power. Therefore the pump power changes v_p which will affect f_0.

In order to measure the offset frequency, the minimum pulse bandwidth needs to be $\sim 30nm$. In this thesis, the bandwidth is too narrow to measure the offset frequency and so the drift in f_0 cannot be directly measured. Therefore, this experiment is in an interesting regime in which the offset frequency has an effect on the power within the EC, but cannot be directly measured in order to have explicit control.

2.2.2 Modematching

Modematching is the process of having the q parameter of the input beam match the spatial eigenmode of the cavity. The importance was discussed briefly in section 2.1.5 in relation to extending the cavity. In the case of an EC, modematching becomes very important when trying to attain the highest possible intracavity power. As the enhancement comes from the addition of many pulses, not only does the temporal phase need to be coherent, but also the spatial phase (see equation 2.29). This then requires the profile of the field at a given point to be identical for every pass in the cavity.

In one plane, modematching using two lenses is simple and will be described here (the more complicated case of two planes with an astigmatic beam will be discussed in Appendix C.2.2). The problem is that the input beam must match the eigenmode of the EC, which is dependent on the cavity geometry. It can be solved by working in two directions simultaneously: one is the real output beam coming from the laser oscillator, while the second is a virtual beam which would be coming from the EC if it were also a laser with an output. A lens of focal length f_a is placed between the two cavities a distance d_a from the laser so that the waist of the real beam matches that of the virtual beam at point d_b. The second lens with focal length f_b is chosen so as to match the radius of curvature

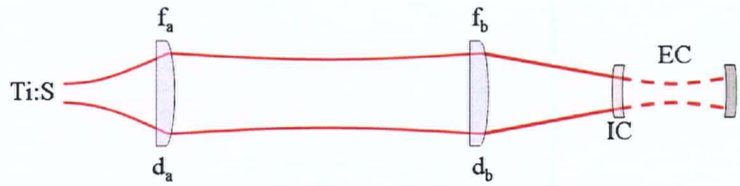

Figure 2.15: Schematic of matching the output of the laser oscillator (solid curve) to the eigenmode of the EC (dashed). The first lens at position d_a is used to match the waist of the beam to that of the eigenmode extending from the EC to point d_b. The focal length of the second lens f_b is used to match the radius of curvature of the beam to guide it into the EC. The beam is now modematched, giving low loss in the first round trip, effectively enhancing the amount of available input power.

of the two beams. The incident beam is now matched to the eigenmode of the EC. Since the divergence of the beam after the first lens depends on both f_a and d_a, there are many solutions for point d_b. Thus, there are also many different lenses with focal length f_b which can be used. This means that a solution to the modematching problem is not unique.

The output beam, which may be astigmatic, is matched to the (also astigmatic) mode inside the EC using a series of lenses. Although it is possible to use a series of cylindrical lenses – lenses which would only affect one plane – each lens has typically close to 10% loss (less if treated with some anti-reflection coating) and so the number of lenses is minimized in order to have the highest power inside the EC. As with spherical mirrors, a lens tilted in the tangential plane by an angle θ changes the focal point in the tangential plane by $f_{tan} = f_0 \cos\theta$ (where f_0 is the focal length of the lens) and the sagittal plane by $f_{sag} = f_0/\cos\theta$ which is key when attempting to minimize the number of lenses. Noticing then that the two planes are coupled through f_0, which is limited by the commercial availability of lenses, the solution becomes non-trivial.

2.2.3 Diffraction inside a Resonator

The current method of retrieving the EUV light is with a thin sapphire plate placed within the EC [5, 6], and is at Brewster's angle for the fundamental beam. Since the polarization of the fundamental beam is linear, the Brewster plate has negligible reflection at the interface. The index of refraction is different for the EUV light however, and so the plate is no longer at Brewster angle and a small amount of light will be reflected. By using a Brewster plate, the high finesse within the EC can be maintained while retrieving the high harmonic. However, this method is inefficient and reflects only $\sim 20\%$ of the EUV light. Also, the transmission through the Brewster plate will inevitably cause some loss, and in a high finesse EC, it is the main source of loss. It is then desired to develop a method of retrieving the EUV without the use of a Brewster plate.

To create a low-loss output coupler, an aperture in one of the focusing mirrors has been suggested [6]. The divergence angle is proportional to the wavelength (see Table 2.2), and so the high harmonic will have a much smaller spot size than the fundamental at the second focusing mirror (see Figure 2.16). Using diffraction theory from reference [25], the goal is to find an optimum aperture size balancing the loss for the fundamental beam while transmitting as much of the high harmonic as possible.

As discussed in section 2.1.5, the field profile inside a cavity is assumed to be gaussian since it is a solution to the paraxial wave equation. However, once a mirror has a finite aperture the profile is no longer gaussian, and so a more general theory is required to calculate the beam profile. One method is to use diffraction theory. This method is much more general in calculating the beam profile inside a cavity since in the ABCD method, a gaussian profile is assumed. Using diffraction theory, the field sees the finite size of the mirrors with the resulting profile being nearly gaussian, which agrees with the ABCD method.

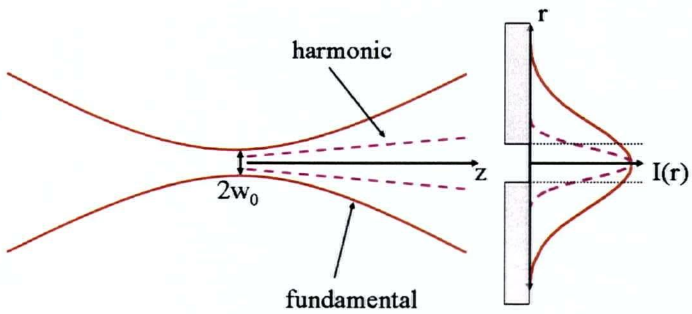

Figure 2.16: The beam divergence for the high harmonic (purple dash) compared to the fundamental (red solid). Due to the shorter wavelength the high harmonic diverges less. By the time the beams have reached the mirror with an aperture (grey rectangles), the difference in the beam waists can be useful for extracting out the EUV while reflecting the fundamental.

However, when an aperture is present in a mirror, the resulting field profile can also be calculated.

The Fresnel number is a unitless length scale and is given as

$$N = \frac{a^2}{\lambda d} \tag{2.54}$$

where a is the radius of the mirror, d is the separation of the mirrors, and λ the wavelength (refer to Figure 2.18). This number relates the cavity dimensions to the wavelength. For a higher N, the field in numerical simulations becomes more sensitive to the cavity dimensions, consequently leading to an extended computation time. The large k for optical wavelengths requires more data points to be taken in the integration (to be discussed below), while a large N can give pseudo-stable solutions, requiring many iterations to converge to the final solution. Qualitatively, this can be described as finding the loss in a cavity using ray optics where the mirrors are large compared to the separation distance. A ray trace can have many bounces within the cavity before being lost even in an unstable resonator (see Figure 2.17).

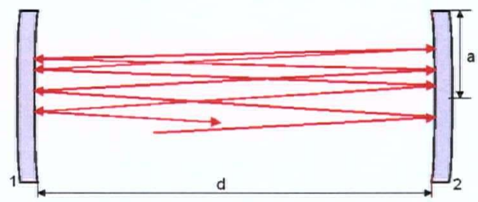

Figure 2.17: Ray trace through a cavity with a large Fresnel number. Many bounces occur within the cavity before finding the stable solution. This causes slow convergence, requires many iterations, and has an extended computing time. Methods of minimizing the Fresnel number are found in order to improve the efficiency of these routines.

The many iterations are a result of the method determining the solution. To find a steady state solution from diffraction theory, a wavefront is introduced to the cavity having some assumed field profile. An initially flat profile is often used to avoid a bias in the final solution. Referring to Figure 2.18, this wavefront is reflected from mirror 1 to mirror 2. However, due to diffraction effects, it no longer has a flat profile, but now has a field that is determined by the reflection of the first mirror. The common cases for this theory have been either planar or confocal [25, 26] cavity designs, and here it is generalized to the case of arbitrary radius of curvature mirrors. The final, steady state profile is the stable field (eigenmode) inside the resonator and the attenuation of each successive round trip for this eigenmode is the loss of the cavity.

The field calculated at each mirror $E_j(r_j, \phi_j)$ for the j^{th} mirror, can be written as

$$E_{j+1}(r_{j+1}, \phi_{j+1}) = \frac{i}{2\lambda} \int_0^a \int_0^{2\pi} E_j(r_j, \phi_j) \frac{e^{-ikR}}{R} \left(1 + \frac{d}{R}\right) r_j \, d\phi_j dr_j \tag{2.55}$$

where λ is the wavelength of light in the resonator, and the other variables are defined in Figure 2.18. Although the cavity can have an arbitrary number of mirrors, many cavity geometries can be reformulated to be linear (see Appendix

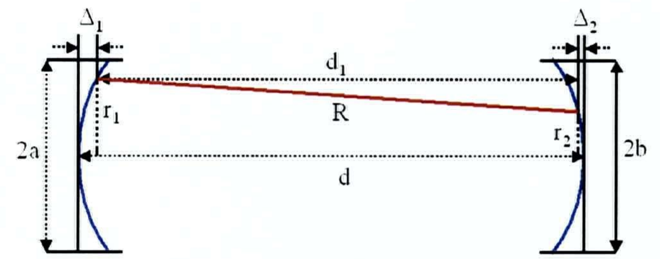

Figure 2.18: The geometry of a linear resonator. The angles ϕ_1 and ϕ_2 in equation (2.55) are the azimuthal angles of the mirrors 1 and 2, respectively, which are separated by a distance d. The distance d_1 is the distance from point with coordinates $(\Delta_1, r_1, \phi_1)$to point with coordinates $(d - \Delta_2, r_2, \phi_2)$. R_1 and R_2 are the respective radii of curvature of the mirrors (represented by the blue curves). Taken from [25]

C.3). From Figure 2.18, it is found that

$$\begin{aligned} R &= \sqrt{d_1^2 + r_1^2 + r_2^2 - 2r_1r_2\cos(\phi_1 - \phi_2)} \\ d_1 &= d - \Delta_1 - \Delta_2 \\ \Delta_1 &= d - \sqrt{R_1^2 - r_1^2} \\ \Delta_2 &= d - \sqrt{R_2^2 - r_2^2} \end{aligned} \tag{2.56}$$

Now in computing the fields, the variables ϕ_1 and ϕ_2 are eliminated in order to simplify the calculation. This can be done using the relation

$$e^{in[(\pi/2-\phi_2]}J_n\left(k\frac{r_1r_2}{d}\right) = \frac{1}{2\pi}\int_0^{2\pi} e^{ik\frac{r_1r_2}{d}\cos(\phi_1-\phi_2)-in\phi}\, d\phi_1 \tag{2.57}$$

where the function J_n is n^{th} order of the Bessel function of the first kind. In order for the $d\phi_j$ integral to be reduced, it needs to be massaged into the form on the right hand side of equation (2.57) which requires a few approximations. First, there is the ratio between the radius of the mirror and the separation of the mirrors. If d/a is large enough to approximate that $R \approx d$ then the product

$$\frac{1}{R(r_1, r_2, \phi_1, \phi_2)} \left(1 + \frac{d}{R(r_1, r_2, \phi_1, \phi_2)}\right) \approx \frac{2}{d} \tag{2.58}$$

As shown in Appendix B, this term can be considered a constant with good confidence as long as $d > a$. To second order, the distance R can be simplified by looking at the definitions for Δ_1 and Δ_2. To this end, it is found that

$$\Delta_i \approx d - R + \frac{r_i^2}{2R_i} + O(r_i^4) \tag{2.59}$$

When substituted into the equation for R, it is found that

$$\begin{aligned} d^2 + r_1^2 + r_2^2 = R_1^2 + R_2^2 + 2R_1R_2d(d - 2(R_1 + R_2)) + \\ r_1^2\left(\frac{d - R_2}{R_1}\right) + r_2^2\left(\frac{d - R_1}{R_2}\right) \end{aligned} \tag{2.60}$$

where all terms containing only constants can be taken out since it is only the intensity which is of interest (recall this is calculating the phase of the field, and the modulus squared will lose this information).

The resulting field is then found to be

$$\gamma_n E_2(r_2) = \frac{i^{n+1}k}{d} \int_0^a E_1(r_1) r_1 J_n\left(k\frac{r_1 r_2}{d}\right) e^{ik\left(\frac{r_1^2}{2d}\left(\frac{d-R2}{R1}\right) + \frac{r_2^2}{2d}\left(\frac{d-R_1}{R_2}\right)\right)} dr_1 \tag{2.61}$$

where the γ_n is to account for the losses in the cavity per round trip for the n^{th} transverse mode. The value of γ_n will reach steady state when the intensity profile also reaches steady state. The loss of the fundamental is the goal of this calculation since we are trying to find an aperture which efficiently passes EUV while still maintaining a high reflectivity for the fundamental beam.

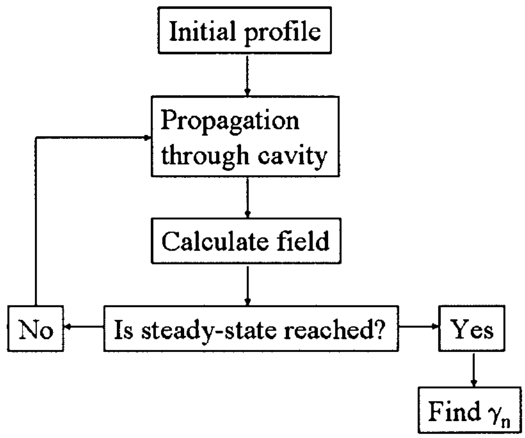

Figure 2.19: The algorithm for calculating a non-gaussian field within a cavity. This algorithm mathematically computes what is physically transpiring in the EC. An initial beam profile enters the cavity, and propagates through the cavity. The field is calculated according to equation (2.61), until a steady-state has been reached. Now the attenuation factor γ_n can be found to give the loss due to an aperture.

2.3 Locking the Laser Oscillator to the Enhancement Cavity

As shown in section 2.2.1, the field must constructively interfere on each round trip to create the intracavity intensity enhancement. In order to do so, either the laser oscillator or the EC must have an active element to compensate for environmental perturbations and cavity length drift. The first requirement is the generation of an error signal sensitive to the relative fluctuations between the laser oscillator and the EC. Such a scheme was developed by Hänsch and Couillaud in 1980 [27]. The essence of this approach is that it measures the relative drift of the cavities via changes in the polarization state of the field measured from the input coupler of the EC. These polarization fluctuations are converted to an electronic error signal used to correct the laser oscillator cavity length.

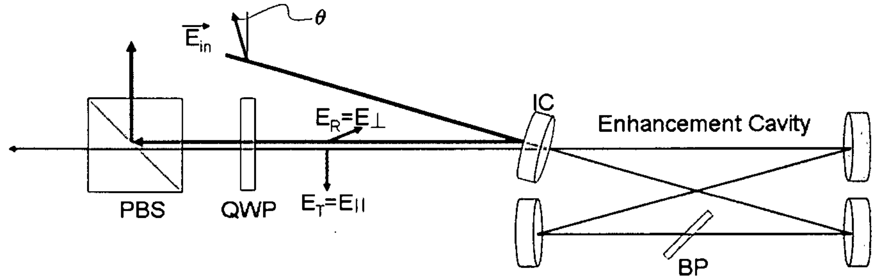

Figure 2.20: The field is incident on the input coupler of the EC with a polarization that is tilted by an angle θ. Due to the Brewster plate (BP) inside the cavity, the perpendicular polarization is attenuated meaning that the intracavity polarization is horizontal. As the intracavity field is transmitted out through the input coupler, it will pick up a phase dependent on the cavity length. This field can be compared with the reflected field, which will have a vertical component. The quarter wave plate (QWP) and the polarizing beam splitter (PBS) are then used to generate the locking signal. The two beams, separated based on their polarizations, are then incident on a balanced photodetector, which takes the difference in the two intensities. Note that the reflected and transmitted beams are collinear, and are separated here for illustrative purposes.

The input beam is a linear combination of horizontal and vertical polarizations (see Figure 2.20). In the plane wave approximation, these can be written as

$$\begin{aligned} E_h^{(i)} &= E^{(i)} \cos\theta \\ E_v^{(i)} &= E^{(i)} \sin\theta \end{aligned} \tag{2.62}$$

where $E^{(i)}$ is the incident field and the angle θ is controlled by a half wave plate (HWP) before the EC. The element inside the cavity which attenuates a certain polarization is the Brewster plate, which is set up so that the least loss is in the horizontal plane. The field that comes off the input coupler is a combination of reflected incident light, and transmitted light which has made many passes through the EC. Similar to the derivation in equation (2.40), for the CW case this field is

$$E_p^r = E_p^{(i)} \left(r_{ic} - \frac{T_{ic} l_p e^{i\phi}}{1 - r_{ic} l_p e^{i\phi}} \right) \tag{2.63}$$

where the loss now depends on the polarization, l_p. T_{ic} is the transmission of the input coupler, with $R_{ic} = r_{ic}^2 = 1 - T_{ic}$, and ϕ is the phase of the field in the cavity. If the loss in the vertical polarization $L_v \gg T_{ic}$ and $l_h = r_{ic}$, then the fields are simplified to

$$\begin{aligned} E_h^{(r)} &= E^{(i)} \cos\theta \left(\sqrt{R_{ic}} - \frac{T_{ic}}{\sqrt{R_{ic}}} \frac{R_{ic} e^{i\phi}}{1 - R_{ic} e^{i\phi}} \right) \\ E_v^{(r)} &= E^{(i)} \sin\theta \sqrt{R_{ic}} \end{aligned} \tag{2.64}$$

Most of the loss comes from the Brewster plate. Due to the geometry of the resonator, the reflected beam and the transmitted beam through the input coupler are completely overlapped and modematched if the cavity has been modematched.

The two polarizations are then passed through a quarter wave plate (QWP) and a polarizing beam splitter (PBS) [16, p 198-200]. The fields are now separated into two arms, given by

$$E_{a,b} = \frac{1}{2} \begin{pmatrix} 1 & \pm 1 \\ \pm 1 & 1 \end{pmatrix} \begin{pmatrix} 1 & 0 \\ 0 & i \end{pmatrix} \begin{pmatrix} E_h^{(t)} \\ E_v^{(r)} \end{pmatrix} \tag{2.65}$$

and so the intensities become

$$I_{a,b} = \frac{1}{4} c\epsilon_0 |E_h^{(t)} \pm i E_v^{(r)}|^2 \tag{2.66}$$

The photodetector receives the two signals and electronically subtracts them and so it is only the difference that is of concern. As shown in section 2.2.1, in the modelocked case the amplitude of the modes of the EC now have an envelope function. Using equation (2.50), the difference of the two signals in a

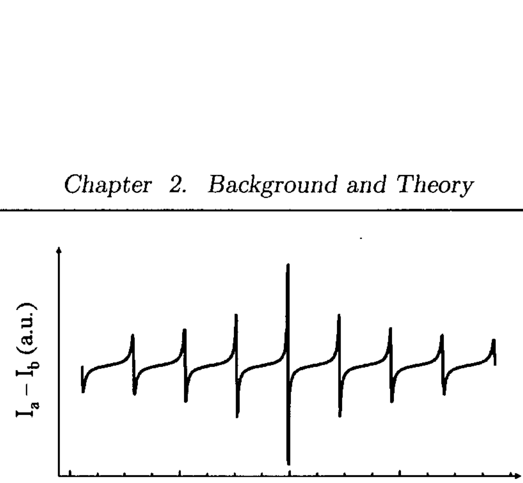

Figure 2.21: Simulated error signal for a multimode EC. As in the case of the maximum attainable intracavity power, there is an envelope which is dependent on the bandwidth of the pulse, and the finesse of the EC. The spacing of the error signal is determined by f_{rep} of the EC and the speed at which the cavity is swept. The absolute position of the error signal is also dependent on the offset frequency, and so the difference in the offset frequencies of the EC and the input field can be measured.

multimode EC becomes

$$I_a - I_b = I^{(i)} \sin(2\theta) \frac{\frac{T_{ic}\pi}{4}\left(\frac{2\mathcal{F}_{eff}(\phi)}{\pi}\right)^2 \sin\phi}{1 + \left(\frac{2\mathcal{F}_{eff}(\phi)}{\pi}\right)^2 \sin^2(\phi/2)} \tag{2.67}$$

The HWP used before the EC adjusts the input polarization θ to tune the signal to noise in the error signal. The effective finesse $\mathcal{F}_{eff}(\phi)$ is now dependent on the matching of the repetition rates and offset frequencies of the laser and EC, as described in section 2.2.1. This then affects the slope of the function as it passes through zero. The lower the finesse means the broader the linewidth of the mode and the lower the slope. Therefore the EC can be made easier to lock to the laser by adjusting the alignment of the comb and EC modes.

In order to have the highest intracavity power, the laser is locked when $p = 0$, that is when the repetition rates and the offset frequencies are matched. This is found from sweeping the laser cavity length to find the largest peak-to-peak difference in the error signal. Then the cavity length is manually adjusted to zoom in on the zero-crossing of the largest difference, and then locking the laser to the EC at this point.

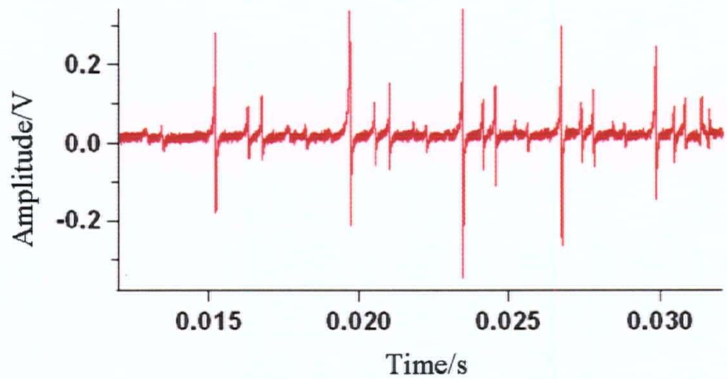

Figure 2.22: The measured error signal. Notice that the signal grows when the cavity lengths are matched. The error signal has the largest amplitude when f_0 and f_{rep} are matched between the laser and the EC (when $p = 0$ in Figure 2.14. The TEM_{00} mode (large peaks) has a non-degenerate frequency with higher order modes (small peaks). The competing modes can be avoided by improving modematching. The spacing is not even as the PZT changes direction (as shown for time $> 30ms$).

The error signal has an interesting property such that the maximum phase that is allowed (ie the maximum amount that the two cavities can drift relative to each other and still be compensated by the electronics) is

$$\phi_{max} = \frac{2\pi}{\mathcal{F}} \tag{2.68}$$

Since the phase $\phi = k\Delta d$ where k is the wavenumber and Δd is the cavity length mismatch, then

$$\Delta d_{max} = \frac{\lambda}{\mathcal{F}} \tag{2.69}$$

This equation dictates that the maximum usable finesse is limited by the stability of the EC. This stability is determined by the external environmental perturbations which can be avoided by using a floating optical table, lead foam, and an isolated cavity design.

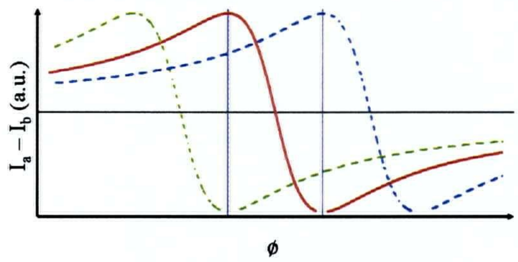

Figure 2.23: The simulated error signal produced for a single linewidth laser. The solid line is exactly matched, while the dashed lines represent the maximum available drift in the cavity with the electronics still able to compensate (represented by the vertical bars). The consequences of this are that the EC length must be stabilized to within a nanometer for a cavity with a finesse of a thousand.

2.4 High-Order Harmonic Generation

High-order harmonic generation is a nonlinear process which uses a strong driving field to give odd-harmonics of the fundamental beam. A pedagogical model for high harmonic generation (HHG) has been developed [28]. This quasi-static model (or three step model) assumes that a valence electron, with the help of the strong driving field, can spontaneously free itself of the Coulomb potential of an atom through tunneling. This atom (now ion) in an intense field does not immediately become separated from its electron, which now follows the applied field lines. Thus, even without effects such as dispersion or defocusing caused by the plasma, the conversion efficiency is necessarily low because of the small tunneling probability.

The second step in this model assumes a classical description of the electron following the electric field of the applied laser, ignoring both the electric field of the ion and the magnetic field of the laser. For linearly polarized light, the motion of the electron in the field is written as

$$x(t) = -\cos(\omega t)x_0 + v_{0x}t + x_{0x}$$

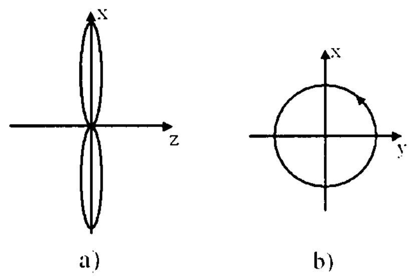

Figure 2.24: Motion of a free electron in a) linearly polarized laser field and b) circularly polarized field. Note that for linearly polarized light the motion is in the xz plane and that for circularly polarized light is in the xy plane. Taken from Ref. [29]

$$v(t) \quad = \quad v_0 \sin(\omega t) + v_{0x} \tag{2.70}$$

where at time $t = 0$ the position and velocity of the electron are set to 0, the same as the position and velocity of the ion. In terms of the field, $x_0 = qE_0/m_e\omega^2$ and $v_0 = x_0\omega$ where E_0 is the field, q the electron charge, m_e is the mass of the electron, and ω the angular frequency of the applied field. The polarization dependence can be seen in Figure 2.24 as the electron in circularly polarized light never returns to the ion, so in order to have HHG the laser field must be linearly polarized.

Now, following the applied field lines the electron returns to the ion with a maximum additional kinetic energy

$$E = 3.2U_p + E_s^0 \tag{2.71}$$

with U_p being the 'ponderamotive potential' – the kinetic energy gained from the field – and E_S^0 is the ionization potential of the atom. The factor of 3.2 in the ponderamotive energy comes from the maximum velocity of the electron attainable in the electric field. The energy E is the maximum photon energy that can be derived from this system.

Once the atom is ionized, the remaining valence electrons experience a new Coulomb potential. Therefore, there remains a probability, although even smaller, that a second electron can tunnel from an ion. The kinetic energy is again equation (2.71), but in this instance the value for E_s^0 has increased. As shown in [30], the highest attainable energy is different for singly charged ions than for neutral atoms.

Chapter 3

Results and Discussion

The theoretical considerations discussed in the previous chapter place many constraints upon the design of the EUV source. In this chapter, experimental results from key components of the source are discussed. This is divided into three sections, the first discussing the high pulse-energy Ti:Sapphire laser seed oscillator, the second describing the mode-matching optics and algorithm used to maximize the coupling to the enhancement cavity (EC), and in the final section the alignment and locking of the EC is discussed. In addition, current results of the EC intracavity power and peak intensity are presented.

3.1 The Ti:Sapphire Oscillator Setup

To attain the highest possible peak intracavity intensity, the oscillator is designed to generate pulses which are an order of magnitude higher in pulse energy than a standard, modelocked $100MHz$ Ti:Sapph laser [9]. One cannot simply increase the pump laser power to obtain a corresponding increase in the Ti:Sapph laser output power. Rather, several effects must be taken into account to generate high energy pulses with high spectral purity from the laser.

3.1.1 Thermal Lensing

In order to achieve the high output power, a V-10 Verdi^{TM} pump laser pumps the Ti:Sapphire laser crystal with $10W$ of CW radiation at a wavelength of $532nm$, and focused onto the crystal with a $10cm$ focal length lens. At this high pump intensity (approaching $10^6 W/cm^2$) thermal lensing in the Ti:Sapph

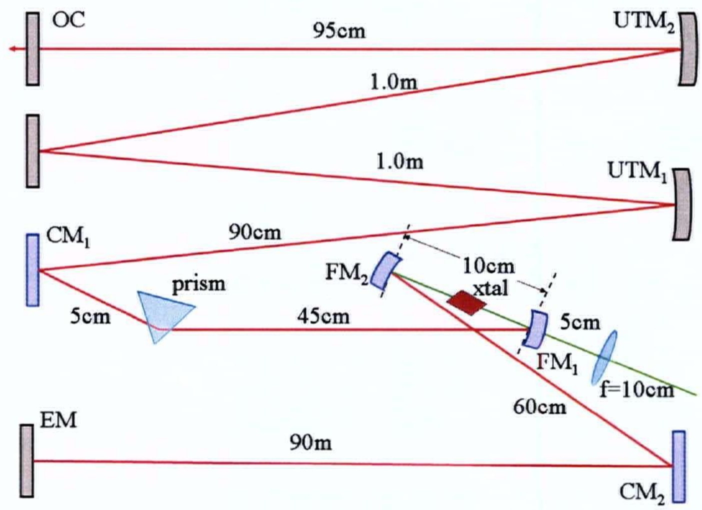

Figure 3.1: The schematic of the $25MHz$ Ti:Sapphire laser. Because of the normal GVD caused by the crystal, anomalous dispersion mirrors are used (blue mirrors CM_i, FM_i) in the cavity. The unity transform mirrors each have a radius of curvature of $2m$, and are separated by $2m$, with the first being $95cm$ from the prism. The prism is located $45cm$ from the focusing mirror FM_1. The output coupler is a 10% transmitting mirror from Layertec with part number 101905. The end mirror (EM) is taken from a MIRA^{TM} laser, and is attached to a piezo-electric transducer for active control of the cavity length. To modematch the pump beam, a $10cm$ focal length lens is placed $5cm$ before FM_1.

crystal can change the stability conditions of the cavity and can decrease the output power. Therefore, the crystal mount must be water cooled. It is found that the most stable operating condition is when the crystal is cooled slightly below room temperature.

3.1.2 The Extended Cavity

The theory of cavity extension in section 2.1.5 is used to find the optimal position of the unity transform mirrors. The cavity is extended to $6m$ and is done with the two mirrors with radius of curvature $R = 2m$ (Layertec part number 103823), separated by a distance of $2m$. The spot sizes of the beam at the prism and at the output coupler are nearly identical, implying the unity transform solution. The fluorescence, which contains the outline of the Ti:Sapph crystal mount, can also be seen at the prism. The fluorescence is flipped both horizontally and vertically at the output coupler.

3.1.3 Dispersion Compensation

In order to achieve pulsed operation, the intracavity dispersion must be carefully tuned. To compensate for the normal dispersion and self-phase modulation that the pulse experiences as it resonates within the oscillator, four chirped mirrors are used within the cavity. The focusing mirrors surrounding the Ti:Sapphire crystal are broadband with anomalous dispersion and have radius of curvature of $10cm$ as in Figure 3.1. These were purchased from Layertec with part number 101568. In addition to these, two more negatively chirped flat mirrors are inserted into the cavity (part number 101515) to give a total mirror dispersion in the cavity of approximately $-560fs^2$ per round trip. The 1/2" end mirror and the 1" cavity mirror, both taken from a Coherent MIRA^{TM} laser, were selected for their high reflectivity at 800nm and their ability to support picosecond pulses. The Ti:Sapphire crystal is $2.3mm$ long, which gives a calculated dispersion of $+266fs^2$ per round trip, leaving approximately $-300fs^2$ of dispersion to be compensated by the prism. To compensate the remaining anomalous dispersion, we use the normal material dispersion of a prism, which is inserted into the beam path via a translation stage. As described in section 2.1.3, this prism also serves a second purpose of limiting the bandwidth of the pulses generated by the Ti:Sapph laser oscillator. Although a CaF_2 prism could be used, the low material dispersion makes it an unsuitable candidate. The spectrum of the output is found to be too broad for our purposes as predicted by Figure 2.5 (b). A low GVD means that we must insert more of the wedge into the beam path, which causes more loss and a low output power (less than $1W$). Also, it is found that a regime known as Q-switch modelocking [31] occurs often, and

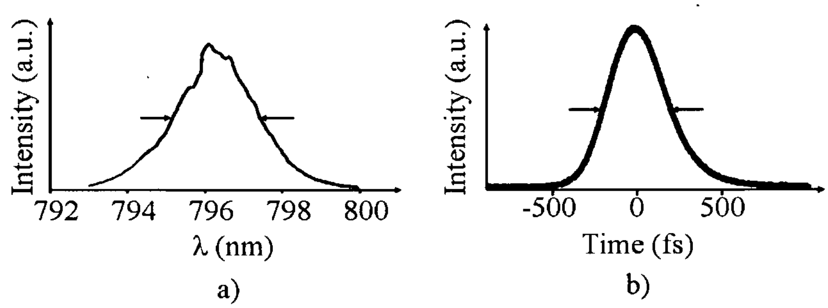

Figure 3.2: a) the Ti:Sapphire laser output spectrum with a FWHM of $2.1nm$; b) the autocorrelation trace of the pulse. The FWHM is approximately $480fs$ for a gaussian pulse, implying that this pulse train is near transform limited. Note that the pulse is not symmetrical, due to an artifact of the autocorrelator and is independent of the pulse.

pulse generation tends to stop on the timescale of an hour. Therefore, an SF10 prism is chosen to limit the bandwidth and finely tune the intracavity dispersion. This prism allows for a bandwidth of $2nm$ when modelocked as shown in Figure 3.2. The position of the prism in the cavity is chosen to minimize its effect on the beam profile. With the SF10 prism in the cavity, the oscillator remains modelocked for an arbitrary length of time, and the average output power has been found to be as high as $1.5W$.

3.1.4 Active Control of the Laser Cavity

In order to lock the laser comb spacing f_{rep} to the free spectral range of the EC, a piezo-electric transducer (PZT) is placed behind the end mirror in the Ti:Sapph laser. Given an applied electric potential, a PZT changes its shape, adjusting the position of the mirror which changes the cavity length. In an ideal case, this is a perfectly translational motion. However, if the PZT does not act as the ideal case then the PZT will induce some (unwanted) tilt to the mirror, which leads to errors in the beam pointing. These pointing issues can have two consequences which are detrimental to locking to the EC. Misalignment in the

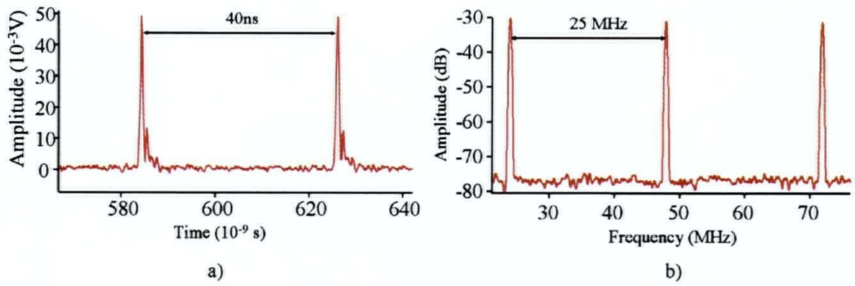

Figure 3.3: a) The stable pulse train created by a $25MHz$ Ti:Sapph mode-locked oscillator. The pulse train can show that the laser is not double pulsing (within the bandwidth of the detector). This occurs when two pulses are generated per pass at the output, and can be more prominent at an output power of $\sim 1W$. b) Radio frequency (RF) spectrum showing the stable repetition rate. Modulations in the spectrum are signs of unstable modelocked operation.

laser affects the pointing of the output beam, which will then not be properly coupled into the EC. Also, with the use of a single prism, horizontal pointing errors will lead to a change in the central wavelength. This effect is amplified if the prism is placed directly in front of the end mirror. Both of the effects need to be avoided in order to have the Ti:Sapph laser tightly locked to the EC.

Sensitivity of the Locking Signal to Noise

As mentioned in section 2.3, the amplitude of the noise that the locking mechanism can compensate is dependent on the finesse of the cavity. This requires that the noise which is written onto the error signal due to environmental perturbations must be very small for a high finesse cavity. It is shown in Figure 3.4 that the vibrations of the table and breadboards are written on to the error signal. These vibrations must be minimized in order to keep the laser locked to the EC. It is found that with the current setup for a $12m$ long laser and EC, a finesse of 300 is the highest possible EC finesse in order for the locking of the laser to the EC to be stable.

A geophone is placed on the Ti:Sapph breadboard to measure the vibrations

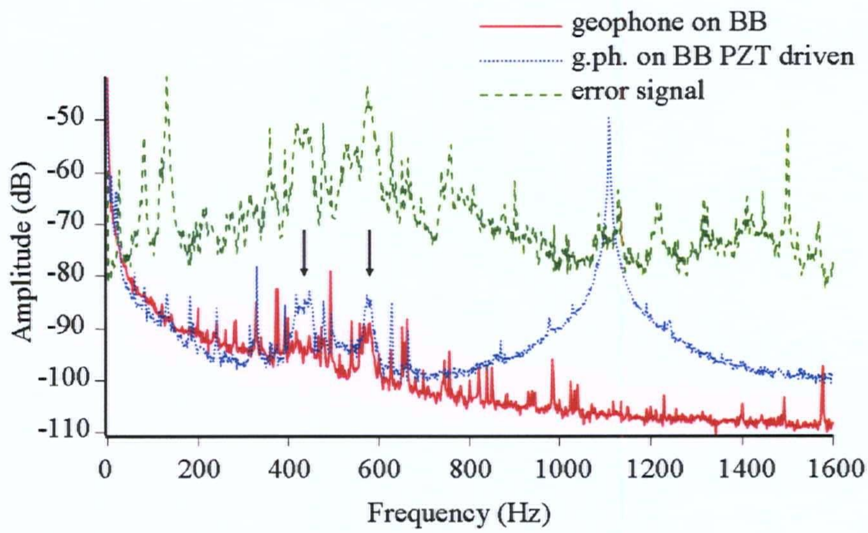

Figure 3.4: Vibration of the optic table written onto the output of the Ti:Sapph laser. A geophone measures the background vibrations of the Ti:Sapph laser breadboard (BB - red solid curve) and when the PZT is driven at $1.1kHz$ (blue dotted line). The noise is also written on to the error signal (green dashed line). See text for details.

when the Ti:Sapph laser is operating with some mid-frequency features arising in the $400 - 600Hz$ range (arrows in Figure 3.4)). When the PZT is driven at $1.1kHz$, there is a corresponding $1.1kHz$ peak in the vibration as measured by the geophone. Additional features are amplified at the mid-frequency range, implying a resonant mode in the table or breadboard. When the EC and Ti:Sapph laser cavities are locked, the error signal also has the characteristic frequencies measured by the geophone. The addition of other features in the error signal is likely due to independent vibrations in the EC breadboard.

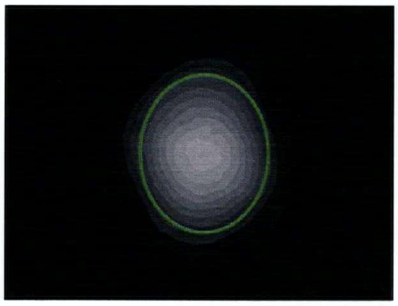

Figure 3.5: The output profile of the Ti:Sapphire oscillator. The green circle approximates the waist in the sagittal and tangential planes. This beam is measured to have sagittal and tangential beam waists of $w_{sag} = 1.61mm$ and $w_{tan} = 1.31mm$ taken a distance of $115cm$ from the output coupler. This predicts the waist at the output coupler to be $w_{0sag} = 183\mu m$ and $w_{0tan} = 227\mu m$.

3.2 Beam Profile Measurement and Modematching

An astigmatic output profile from the laser must be matched to the EC, which also supports a different astigmatic eigenmode. This procedure is not a trivial task. Using frame grabbing software and a CCD camera, the beam waist can be accurately measured in both planes. Taking these images and fitting them to a nonlinear solver routine, a gaussian profile can be fit for the two planes, allowing for an accurate measurement of the beam waist in each plane. By measuring the waist at various distances from the laser, the radius of curvature from the output coupler can be found as well (ideally it is infinite in both the sagittal and tangential planes since the output coupler is flat). This then gives the q_{out} parameter at the output of the laser.

Errors are introduced because of the small CCD chip size, and that the CCD camera is designed for low ($\mu W/cm^2$) intensity. Since we are shining a beam with output intensity $> 1000W/cm^2$ onto the CCD chip, it must be greatly attenuated before entering the camera. A piece of uncoated glass reflects approximately 5% of the beam to reduce the intensity by a factor of 20. The light from the oscillator is horizontally polarized, and so a rotatable polarizing beam splitter can be used to attenuate much of the signal. Also, neutral density filters from Thorlabs are placed before the camera. Since the filters are absorptive, they create a mild thermal lensing effect when placed before other attenuating optics.

With the q_{out} parameter of the output beam now measured, we must match this with the q_{EC} parameter of the EC. The q_{EC} however, is calculated based on the ABCD matrix method. In order to do this, several measurements within the EC must be taken. These are the distances from the input coupler to the focusing mirrors, their respective angles of incidence, and the total cavity length. Based on these measurements, the optimum (most stable) focusing mirror separation can be found. A stable cavity configuration will now predict a q_{EC} for the tangential and sagittal planes. Matching these parameters to q_{out} is done with a pair of lenses. The calculated q_{EC} is put into an algorithm that was developed for this thesis which is given in Appendix C.2.2. This algorithm takes the radius of curvature and waist of the output beam from the oscillator, and matches it to the eigenmode of the EC using a list of lenses available to the user.

If silver mirrors and lenses without AR coating are used to guide the beam, the input power can decrease by over 20%. To avoid this additional loss, 1" mirrors from Newfocus with high reflectivity are used (part number 5102) and the lenses have an anti-reflection (AR) coating (Newport coating AR.16). The lenses used are dependent on the minimum waist within the EC. As an example, for a minimum waist within the EC of $8\mu m$, a pair of lenses with focal lengths $-100mm$ and $300mm$ were placed $223mm$ and $451mm$ respectively from the Ti:Sapph laser OC. The total propagation distance from the laser to the EC is

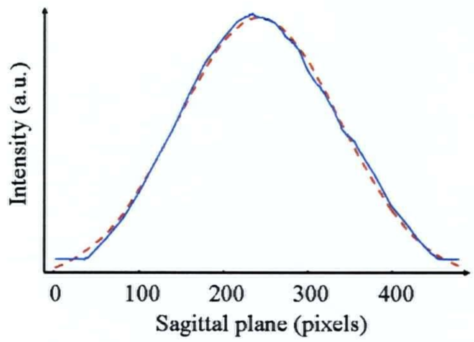

Figure 3.6: The fit of a gaussian (red dash) to the beam profile (blue solid). The fit parameters give a waist of 193 pixels or $1.21mm$. This accuracy in the measurement of the beam profile allows for improved modematching methods.

$1.7m$.

3.3 The Enhancement Cavity

3.3.1 Setup of the Enhancement Cavity

In order to couple all of the modes from the laser into the EC, the total length must be $12m$ to match the repetition rate of the laser. It is a ring-cavity so that the field travels in one direction within the EC. Because of the absorption of EUV light in air, the EC is designed within a vacuum chamber which is to be evacuated to $\sim 50mTorr$. The breadboard, which measures 6" long by 6' wide, is clamped directly to the vacuum chamber, which did not damp vibrations from the environment. Due to these vibrations, the finesse is spoiled by using a 1% input coupler to allow for locking the laser to the EC.

3.3.2 Alignment of the Enhancement Cavity

The EC is difficult to align for two key reasons. First, it is $12m$ long with several fold mirrors. Second, the stability region for the separation of the focusing mirrors is only several hundreds of microns. To optimize the intracavity power, a systematic method of alignment is required. Since the input beam is pulsed,

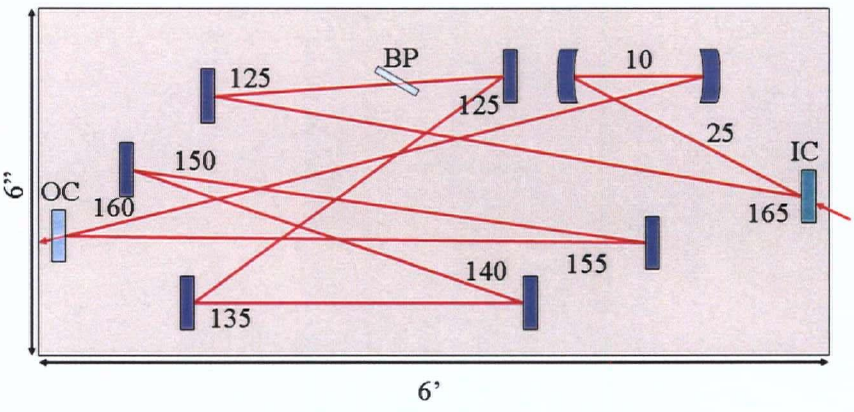

Figure 3.7: A schematic diagram of the EC. In order for the cavity to match the length of the Ti:Sapph laser, 10 mirrors in total are used. Each mirror is highly reflective ($R_{mir} = 99.994\%$) in order to have a high finesse cavity, except for the input coupler (IC) and output coupler (OC). The transmission of the IC is 0.96% and the OC is 0.09%. The OC is designed to account for dispersion within the cavity, and has $\sim -60fs^2$ GDD. The two focussing mirrors have a radius of curvature of $10cm$, and minimum waist of the beam is $7\mu m$. The breadboard measurements are in imperial units, and all other measurements are in centimeters. The Brewster plate is not placed near the focal point.

there will only be interference effects that are observable when the cavity lengths are matched to within $\sim c\tau$ where c is the speed of light, τ is the pulse duration. If the resonator and oscillator lengths are mismatched enough so that the interference effects are no longer visible, the alignment process becomes much simpler. Since there are no interference effects, cavity length drift does not affect the power or spot size. Using a CCD camera as well as a powermeter to detect the leakage behind a weak output coupler as in Figure 3.7, the cavity can be properly aligned. This process can even be used to optimize the modematching lenses.

The average output power through one pass of the EC is $P_0 T_{ic} T_{oc}$ where P_0 is the input average power, and T_{ic} and T_{oc} are the input and output coupler transmission coefficients. By averaging over all the possible modes of the EC, it is found that when the cavity lengths are mismatched, the maximum attainable output power is

$$P_{max} \approx P_0 T_{ic} T_{oc} \frac{\mathcal{F}}{2\pi} \tag{3.1}$$

for high finesse ($\mathcal{F}$) cavities.

The repetition rate of the extended laser oscillator is $25MHz$, implying that the cavity length is approximately $6m$ as a linear cavity. The EC is a ring cavity so it must be $12m$ in length. Because these cavities are so long, it becomes increasingly difficult to match the lengths without some method of accurate measurement. Initially, the simplest method found is to physically measure the mirror separation within the EC to find a rough estimate of the cavity length. In order to match the cavity length of the oscillator to that of the EC, the laser output coupler is mounted on a translation stage. With a remote actuator capable of $50nm$ steps (NewFocus Picomotor 8351), the laser cavity length can be finely adjusted, with a range of a centimeter. Once the two cavity lengths are matched to within the pulse length $\Delta L \approx c\tau$ (where τ is the pulse duration), interference effects from the field are observed.

To detect the interference of the fields, two methods can be employed. One uses a fast spectrum analyser (USB2000 Miniature Fiber Optic Spectrometer from Ocean Optics) placed behind the OC of the EC. The spectrum changes from that seen in Figure 3.2 (a) to having a modulated envelope. A fast spectrum analyser is required to show the change in the spectrum as the EC length is changed. Another is using a CCD camera. The interference causes bright and dark fringes once the two lengths are matched.

3.3.3 Measurement of the Enhancement Cavity Finesse

In order to predict the enhancement within the cavity, the finesse needs to be measured. Recall that the intracavity photon lifetime τ_p is related to the finesse by

$$\tau_p = \frac{\mathcal{F}}{2\pi\nu_{FSR}}$$

The finesse can be measured using the techniques developed in references [32, 33]. This technique uses the resonance of the EC as a gate. The end mirror PZT is driven with a sinusoidal signal, sweeping the cavity length of the Ti:Sapph laser. On resonance, the EC matches the modes of the input laser field at time t_0 and has a high power. Now as the laser cavity length is changed slightly, the comb elements of the laser field are no longer resonant within the EC, effectively reflecting any further light. Thus, the light that is leaking out of the EC off resonance must have been from when the two cavities were matched. The intensity of the light then follows the decay curve

$$I(t) \sim I_0 e^{-t/\tau_p} \tag{3.2}$$

and so finding the slope of $ln[I(t)]$ will give the photon lifetime. When the cavity is swept slowly - a relative term involving both the finesse and the cavity length - there are pronounced features to the decay due to temporary interference effects of the field. In order to avoid these features, the velocity of the sweeping mirror must satisfy

$$v \gg \frac{c\lambda}{L_0 \mathcal{F}^2} \tag{3.3}$$

for the intensity to follow the exponential decay (see Figures 3.8 and 3.9 for comparison). In this expression, L_0 is the total cavity length and λ is the central wavelength.

3.3.4 Current Enhancement Cavity Buildup Results

Using a 1% input coupler and a 0.1% output coupler, the finesse is measured to be 290. This predicts a maximum enhancement factor of $\sim$ 100. The amount of light that was coupled into the EC was $720mW$. Once the Ti:Sapph laser

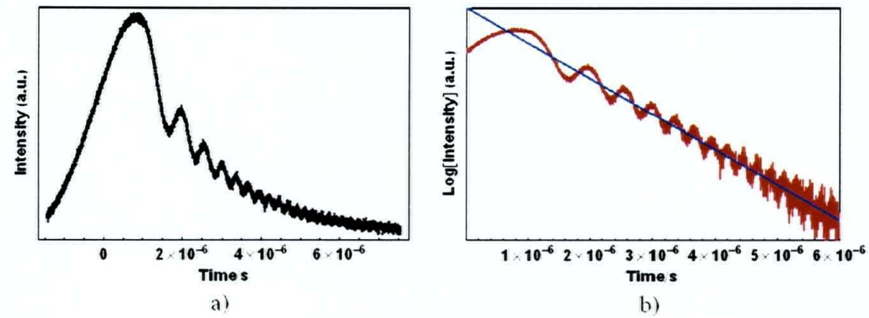

Figure 3.8: a) Output signal through the EC from the cavity ring-down technique. Using an input coupler of 1%, an output coupler of 0.1% and a Brewster window, the finesse is expected to be $\sim$ 300. The PZT is driven at a frequency of $70kHz$. b) Logarithm of the cavity ringdown, and the fit. The slope is related to the photon lifetime. Signal taken with NewFocus 1801 Photoreceiver. This example gives a finesse of 290.

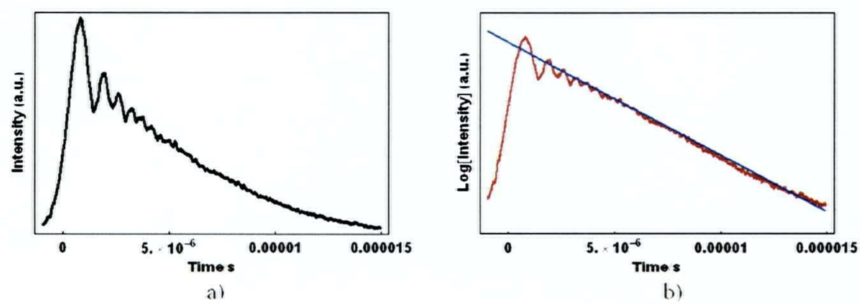

Figure 3.9: a) The ringdown measurement of a high finesse ($\mathcal{F}$ = 4000) $150MHz$ cavity and b) the exponential decay. Using a low-loss input coupler ($R_{ic} = 99.9\%$) and highly reflective mirrors ($R_{mir} = 99.994\%$) the photon lifetime is on the order of tens of microseconds. Notice that the sinusoidal modulation is reduced even though the PZT is driven at only $15kHz$.

was locked to the EC, the intracavity power was $34.1W$, or $47.4\times$ the initial input power. This gave a calculated peak power at the focal point to be $\sim 4 \times 10^{12} W/cm^2$, or to within a factor of 2 of the required intensity for HHG. Routes toward exceeding this threshold intensity are discussed in the next chapter.

Chapter 4

Conclusions and Future Work

In this thesis several significant steps toward the development of a small-scale, high-photon flux source of EUV radiation suitable for high precision spectroscopy are demonstrated. In order to obtain the high peak intensity required for generation of EUV photons via high harmonic generation, a passive enhancement cavity (EC) seeded by a custom-built modelocked Ti:Sapphire laser is employed. The laser is designed to generate a train of near-transform limited $480fs$ ($2.1nm$), $60nJ$ pulses. To achieve this performance level, the laser cavity is stretched to $6m$ in length via a unity mode transform mirror set and a single SF10 prism is used as both an intra-cavity spectral filter and as an adjustable dispersion compensation element. Maximizing coupling of the laser-generated seed into the EC is accomplished by using an algorithm (written in *Mathematica*) which matches the astigmatic mode of the laser output with the (different) astigmatic eigenmode of the EC via a pair of lenses. After properly mode-matching the laser to the EC and locking the two cavities together, an enhancement factor of 50 is obtained giving $4 \times 10^{12} W/cm^2$. This, unfortunately is not enough for ionization.

Several factors which limit the enhancement have also been investigated, and in future work will be addressed. In order to lock the Ti:Sapph laser oscillator to the EC, the active element is a mirror with a PZT to adjust the cavity length of the Ti:Sapph laser. The pointing issues which arise from the PZT misalign the laser. The PZT can be either moved to the EC, or another device to effectively change the cavity length such as an EOM may be employed. The locking mechanism is also very sensitive to vibrations, and so both the Ti:Sapph laser and EC must be isolated from environmental perturbations. Improvements on the vibration isolation of the cavities will allow us to increase the finesse to > 1000, thereby increasing the intracavity intensity to more than $10^{13} W/cm^2$.

Bibliography

[1] X. Zhang, A. R. Libertun, A. Paul, E. Gagnon, S. Backus, I.P. Christov, M.M. Murnane, H.C. Kapteyn, R.A. Bartels, Y. Liu and D.T. Attwood, "Highly coherent light at 13 nm generated by use of quasi-phase-matched high-harmonic generation," Optics Lett. **29**, 1357-1359, (2004)

[2] E.A. Gibson, A. Paul, N. Wagner, R.Tobey, D. Gaudiosi, S. Backus, I.P. Christov, A. Aquila, E.M. Gullikson, D.T. Attwood, M.M. Murnane, H.C. Kapteyn, "Coherent soft X-ray generation in the water window with quasi-phase matching," Science **302**, 95-98, (2003)

[3] A. L'Huillier and Ph. Balcou, "High-order harmonic generation in rare gases with a 1-ps 1053-nm laser," Phys Rev Lett. **70**, 774-777, (1993)

[4] N. A. Papadogiannis, B. Witzel, C. Kalpouzos, and D. Charalambidis, "Observation of Attosecond Light Localization in Higher Order Harmonic Generation," Phys Rev Lett. **83**, 4289-4292, (1999)

[5] C. Gohle, T. Udem, M. Herrmann, J. Rauschenberger, R. Holzwarth, H.A. Schuessler, F. Krausz and T. Hänsch, "A frequency comb in the extreme ultraviolet," Nature **326**, 234-237, (2005)

[6] R.J. Jones, K.D. Moll, M.J. Thorpe and J. Ye, "Phase-Coherent Frequency Combs in the Vacuum Ultraviolet via High-Harmonic Generation inside a Femtosecond Enhancement Cavity," Phys Rev Lett. **94**, 193201, (2005)

[7] A. Bartels, C. W. Oates, L. Hollberg, and S. A. Diddams, "Stabilization of femtosecond laser frequency combs with subhertz residual linewidths," Optics Lett **29**, 1081-1083, (2004)

[8] S.T. Cundiff, "Phase stabilization of ultrashort optical pulses," J. Phys D: Appl Phys. **35**, 43-59, (2002)

[9] Fortier T.M., PhD thesis, U of Colorado, (2004)

[10] Milonni P.W., Eberly J.H., *Lasers*, John Wiley and Sons, (1988)

[11] Brandi F., PhD Thesis, Vrije Universiteit Amsterdam, (2004)

[12] T. Kasuya, T. Suzuki, and K. Shimoda, "A Prism Anamorphic System for Gaussian Beam Expander," Appl Phys **17**, 131-136, (1978)

[13] http://www.cvilaser.com/Common/PDFs/Dispersion_Equations.pdf

[14] R. L. Fork, 0. E. Martinez, and J. P. Gordon, "Negative dispersion using pairs of prisms," Optics Lett **9**, 150-152, (1904)

[15] S. H. Cho, F. X. Kärtner, U. Morgner, E. P. Ippen, and J. G. Fujimoto, "Generation of 90-nJ pulses with a 4-MHz repetition-rate Kerr-lens mode-locked Ti:Al2O3 laser operating with net positive and negative intracavity dispersion," Optics Lett **26**, 560-562, (2001)

[16] Saleh B.E.A., Teich MC, *Fundamentals of Photonics*, John Wiley and Sons, (1991)

[17] Siegman A.E., *Lasers*, University Science Books, (1986)

[18] R.J. Jones and J. Ye, "Femtosecond pulse amplification by coherent addition in a passive optical cavity," Optics Lett **27**, 1848-1850, (2002)

[19] E.O. Potma, C. Evans, X.S. Xie, R.J. Jones and J. Ye "Picosecond-pulse amplification with an external passive optical cavity," Optics Lett. **28**, 1835-1837, (2003)

[20] R.J. Jones and J. Ye, "High-repetition rate coherent femtosecond pulse amplification with an external passive optical cavity," Optics Lett **29**, 2812-2814, (2004)

[21] Hammond TJ, Jiang J, Jones DJ, *Phase Stabilization of Modelocked Ti:Sapphire Lasers*, APSNW, (2004)

[22] A. Ashkin, G. D. Boyd, and J. M. Dziedzic, "Resonant Optical Second Harmonic Generation and Mixing," IEEE J. Quant. Electronics **2**, 109-124, (1966)

[23] Jones R.J., PhD Thesis, U of New Mexico, (2001)

[24] L. Xu, Ch. Spielmann, A. Poppe, T. Brabec, F. Krausz, and T. W. Hänsch, "Route to phase control of ultrashort light pulses," Optics Lett. **21**, 2008-2010, (1996)

[25] A.G. Fox and T. Li, "Resonant Modes in a Maser Interferometer," Bell Syst. Tech. J **40**, 453-488, (1979)

[26] A. Waksberg, "Losses of aperture coupling resonators for extended range of Fresnel numbers," Int J Inf & Summill W., **23**, 635-634, (2002)

[27] T. W. Hänsch and B. Couillaud, "Laser frequency stabilization by polarization spectroscopy of a reflecting reference cavity," Opt. Commun., 35, 441 -444, (1980)

[28] P.B. Corkum, "Plasma Perspective on Strong-Field Multiphoton Ionization," Phys Rev Lett. **71**, 1994-1997, (1993)

[29] Boyd RW, *Nonlinear Optics*, Elsevier, (2003)

[30] J.L. Krause, K.J. Schafer and K.C. Kulander, "High-Order Harmonic Generation from Atoms and Ions in the High Intensity Regime," Phys Rev Lett. **68**, 3535-3538, (1992)

[31] Q. Xing, W. Zhang and K.M. Yoo, "Self-Q switched self-mode-locked Ti:sapphire laser," Optics Comm. **119**, 113-116, (1995)

[32] K. An, C. Yang, R.R. Dasari and M.S. Feld, "Cavity ring-down technique and its application to the measurement of ultraslow velocities," Opt Lett. **41**, 1068-1070, (1995)

[33] J. Morville, D. Romanini, M. Chenevier and A. Kachanov, "Effects of laser phase noise on the injection of a high-finesse cavity," Applied Opt. **41**, 6980-6990, (2002)

Appendix A

The Ti:Sapphire Laser

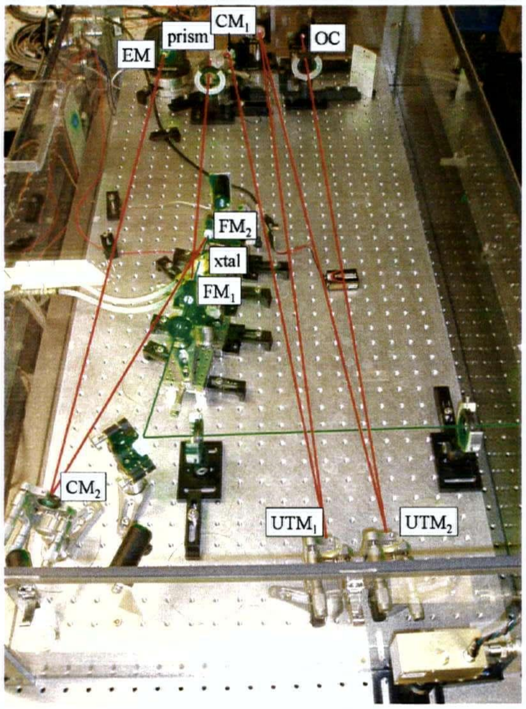

Figure A.1: The Ti:Sapphire laser oscillator designed and built for this thesis. It is pumped by a Verdi V-10 at $532nm$. See Figure 3.1 and the surrounding discussion for details.

The Ti:Sapphire laser used in this experiment is a home-built oscillator. The output of the laser is typically $> 1W$, but when the system has been run in modelocked operation for an extended period of time (several weeks) the power can decrease by up to 20%. However, the beam profile, central wavelength, and bandwidth of the output all remain constant. In order to regain the lost power, the Ti:Sapphire crystal can be translated perpendicular to the pump beam and the focusing mirrors readjusted.

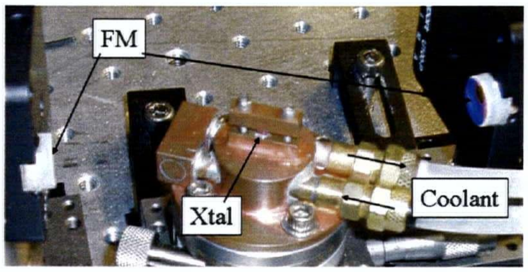

Figure A.2: The mount used in this experiment for the Ti:Sapphire crystal. FM are the two chirped focusing mirrors.

The mount used for the Ti:Sapphire crystal is also an original design. It is made of copper to conduct heat away from the crystal. The tubes used for cooling the crystal mount are lower than the beam in the cavity, which allows for the crystal to be located in the middle of the cavity.

Appendix B

Approximation of d/a

The dependence of R in equation (2.58) on r_1, r_2, ϕ_1 and ϕ_2 at large distances can be simplified in the denominator as $R \approx d$. However, for large mirrors with short focal lengths this approximation is no longer valid. Figure B.1 shows when the separation is less than the mirror size, then this approximation is not justified. The numerical calculation of R is computationally slow, and so avoiding this calculation can speed up the algorithm used to calculate the field in a resonator.

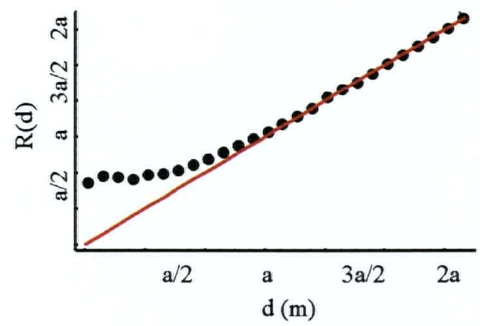

Figure B.1: Here small d is investigated for $2a = 1/2''$ mirror. The numerical calculation of R (circles) and the approximation $d = R$ (solid line). From this it is assumed that as long as $d > a$ then this approximation is valid.

Appendix C

Codes

All codes are written in *Mathematica*. The shebang statement declaring the used packages and removing variables from memory are not displayed. The programmes are transcribed for this thesis, however *Mathematica* uses many of its own shortcut keys and symbols which do no transcribe well into *Latex*.

C.1 Unity Transform Mirror Calculation

The q parameter of the short ($82MHz$) cavity has already been calculated at this point. We are attempting to match the q of the short cavity to that of a longer one, and need to solve equation (2.37) which contains 5 parameters. Since we know that we want a cavity length of $6m$ (instead of $1.8m$), the total distance $D = d_1 + d_2 + d_3$ will be $4.2m$. We can further constrain these distances by requiring $R_1 = R_2$, and so $d_1 = d_3$ by symmetry. Now our equation is only a function of 2 parameters, the radius of curvature of the mirrors and their separation.

The matrices are given as follows, with d2 is the intra mirror distance.

```
Md1={{1,d1},{0,1}};
Md2={{1,d2},{0,1}};
Md3={{1,d3},{0,1}};
MR1={{1,0},{-2/r1,1}};
MR2={{1,0},{-2/r2,1}};
```

The resulting final ABCD matrix of the extension and the coefficients are

```
Mf=Md1.MR1.Md2.MR2.Md3;
AA=Mf[[1,1]];
BB=Mf[[1,2]];
```

```
CC=Mf[[2,1]];
DD=Mf[[2,2]];
```

If we assume that R1=R2 (for this laser we are using $2m$ radius of curvature mirrors), then d1=d3 by symmetry. So then this is only a function of d2 since the total extension distance disttotal is known.

```
R1=R2=2;
disttotal=4.2;
d1=d3;
d3=(Tdist-d2)/2;
```

So the beam waist squared is given as

```
w02=(-\[ImaginaryI]*lambda*BB)/(pi*Sqrt[(AA+1)*(AA-1)])
/.{Tdist->disttotal,lambda->800*10^-9};
```

with the minus sign coming from the q definition. The q in complex, so depending on the definition of the gaussian beam, the imaginary part is either positive or negative. Also the two roots of q are positive and negative. If we just square w02, then we don't need to worry about this minus sign anyways.

Unfortunately we do need to assume some previous beam waist (since we are matching the original q). We will use half a millimeter for this example.

```
w0short=500*10^-6;
dist2=Solve[w0short^4==w02^2,d2];
```

We normally get some complex solutions and a real solution for our d_2. We just want the real solution.

```
d2tab=d2/.dist2//Sort
d2=Select[d2tab,#\[Element]Reals&][[1]]
Out[491]=  2.10172
```

Now double check that it matches the original beam waist.

```
Sqrt[w02]//Chop
Out[492]=  0.0005
```

And the other two distances are

```
d1/.Tdist->disttotal
d3/.Tdist->disttotal

Out[493]=
1.04914

Out[494]=
1.04914
```

So now we have found, for a given pair of mirrors of radius of curvature $R_1 = R_2 = 2m$, the distance that they are separated and their positions within the cavity. It is dependent on the original cavity design which dictates the original beam waist at the output coupler.

C.2 Beam Characterization and Guiding to the EC

C.2.1 Beam Profile Measurement

The built-in nonlinear fitting routine in *Mathematica* can be used for fitting a function to a gaussian. Importing the image is done here. If many images are needed, then name them something in increasing integers. Here 10 images are used as an example. The `ToString` function is used to import the $\mathtt{i}^{th}$ image to `figname`. It is important that the camera is not moved between images, but the attenuators before the camera may. The imported images are all added together to get an average to improve the measurement of the beam waist.

```
img = 0;imax=10
For[i = 1, i <= imax,
    strI = ToString[i];
    figname = StringJoin["c:\\profiledirectory\\
     profile", strI, ".jpg"];
    importedimage = Import[figname, "jpg"];
    img += importedimage[[1, 1]];
    i++];
```

The next part is used to find the beam centre since positioning of the beam on the camera face is not always the same. The image is then sliced in the horizontal and vertical planes at this maximum value.

```
brightest = Max[img];
maxval = Mean[Position[img, brightest]] // Round;

maxsectionhor =
    Table[{i, img[[maxval[[1]], i, 1]]}, {i, 1,
    Length[img[[1]]]}];
maxsectionvert = Table[{i, img[[i, maxval[[2]],
1]]}, {i, 1, Length[img]}];
```

The nonlinear solving routine finds the gaussian fit. This routine needs some initial guesses.

```
fittingtan = NonlinearFit[maxsectionhor,
    AA*Exp[-2*(x - x0)^2/wx^2] + BB, {x},
    {{x0, Length[img[[1]]]/2}, {AA, 255*imax},
     {wx, 150}, {BB, 0}}]
```

From this, the waists in the horizontal and vertical planes are found in pixels. For this experiment, we had a Sony SuperHAD CCD camera with 640×480 resolution, and a $4 \times 3mm$ chip. A larger chip would allow for measures farther from the output coupler since at $3mm$ the chip size is comparable to the beam spot size within a few meters from the output coupler.

C.2.2 Modematching

The following code is the modematching algorithm. Taking the beam q parameters for tangential and sagittal planes from the laser in the measurements done above, these are then used to match to the calculated eigenmode of the EC.

The functions are separated into real and imaginary parts, as well as tangential and sagittal. The imaginary part relates to the waist, and the real to the radius of curvature, and are both required to match to the mode of the EC. The waist is matched first, and then the radius of curvature, and by separating the real from the imaginary this becomes more apparent. Although a 4×4 matrix can be used for astigmatic beams, the planes are separated since it simplifies the solving routine used by *Mathematica*.

The `qinv` functions represent the inverse q parameters, which are

$$\frac{1}{q} = \frac{1}{R} - \frac{i\lambda}{\pi w^2}$$

for both the tangential and sagittal planes. This is also represented by

$$\frac{1}{q(d_1)} = \frac{A + B/q(d_0)}{C + D/q(d_0)} \tag{C.1}$$

where A, B, C, and D are the matrix values. From here, all the (complex) functions are then split into real and imaginary parts for reasons explained above. The names of the functions in this programme represent where the beam is in relation to the lenses and EC. For example, `imqinvd1f1d2tan` is the imaginary part of tangential plane of q^{-1} after it has propagated a distance `d1` and passed through lens `f1`.

The following is the list of lenses available. This is the main reason that this programme can take an appreciable amount of time to run, because of the 200 possible combinations. If only a few lenses are available or if only a few solutions are needed to be found, this can substantially decrease the time for this programme to run. Due to the complications of the astigmatism, not every lens pair will find a solution, and not every solution will be practical. Better solutions include those with smaller angles of the lenses, as well as practical lens positions.

```
lens1tab={-200,-150,-125,-100,-75,75,100,125,150,175,200,250,
300,500};
lens2tab={-200,-150,-125,-100,-75,75,100,125,150,175,200,250,
300,500};
```

The total distance between the laser OC and the cavity IC

```
dtot=2000;
```

The initial guesses for the position of lens 1, with more guesses being more accurate, but slower. I recommend at least 5 steps, ending about 2/3 of `dtot` since there needs to be sufficient space for the second lens. **thresh** is the threshold for the ones that seem to have no solution, and most of the solutions have a value < 100. `fac` is the amount of overstepping of the valid solution boundaries to do for the next iteration. **\[Theta]1max** is the biggest angle (in degrees) that will be allowed for the first lens with it returning a solution.

```
d1init=200;
d1final=1750;
numstep=7;
thresh=150;
fac=2/3;
\[Theta]1max=45;

d1step = (d1final - d1init)/numstep // N
dist1tab = Table[i, {i, d1init, d1final, d1step}] // N

f1t = lens1*Cos[\[Theta]1]; f1s = lens1/Cos[\[Theta]1];
totalsols = 0;
```

The rest calculates the solutions for the lenses given. It is all entered in one cell in *Mathematica*.

```
For[f1val = 1, f1val <= Length[lens1tab],
  For[f2val = 1, f2val <= Length[lens2tab],
    lens1 = lens1tab[[f1val]];
    lens2 = lens2tab[[f2val]];
    errtab = {};
    gooddist1 = {};
    newdist1tab = {};
    errroot = 0;
    zerocross = 0;
```

The first attempt just scans to see if there are solutions. If there are, and if they are within the threshold, then we try again using the boundaries given by the first try to get more data points to fit the error curve. When the error = **ans-lens2** crosses through zero, we have a solution. The third attempt uses the zero of the error as the solution.

```
For[attempt = 1, attempt < 4,
   If[attempt == 1, numd1 = Length[dist1tab]];
```

```
If[attempt == 2, numd1 = Length[newdist1tab]];
If[attempt == 3, numd1 = 1];
numreals = 0;

For[d1val = 1, d1val <= numd1,
If[attempt == 1, dist1 = dist1tab[[d1val]]];
If[attempt == 2, dist1 = newdist1tab[[d1val]]];
If[attempt == 3, dist1 = errroot];
```

Finding the solutions. This uses a built - in routine, which matches the real output beam waist from the laser at **d2** with the virtual beam waist from the EC eigenmode.

```
sol1 = Solve[{imqinvd1f1d2tan[dist1, lens1*Cos[ang1],
d2] == imqinvcavtan[dist1 + d2],
        imqinvd1f1d2sag[dist1, lens1/Cos[ang1], d2]
         == imqinvcavsag[dist1 + d2]}, {d2, ang1}];
```

We join the solutions to form a two - dimensional array of the **d1**'s and **θ1's**.

```
grosssols = Join[Transpose[{d2 /. sol1, ang1 /. sol1}]];
```

Then we select the ones that have real solutions, and have positive **d1**'s and $\theta 1 < \theta 1 max$ degrees.

```
realsols = Select[grosssols, # \[Element] Reals &&
#[[1]] > 0 && #[[2]] > 0 && #[[2]]
 < \[Theta]1max/180*\[Pi] &];
dist2 = realsols[[1, 1]];
\[Theta]1 = realsols[[1, 2]];
```

Now if we have some real solutions, then we go into this part

```
If[Length[realsols] > 0,
     numreals++;(*counts the number of times we attempt
     this routine*)
     f1t = lens1*Cos[\[Theta]1] // Chop;(*tangential
     and sagittal focal lengths for the first lens*)
     f1s = lens1/Cos[\[Theta]1] // Chop;
```

The next solution is for the radius of curvature at **d2**, and which lens is needed to match them. The **tan** and **sag** planes are independent right now.

```
    fts =
      Solve[{reqinvd1f1d2f2d3tan[dist1, f1t, dist2, f2tan, 0]
       == reqinvcavtan[dist1 + dist2 + 0],
          reqinvd1f1d2f2d3sag[dist1, f1s, dist2, f2sag, 0] ==
            reqinvcavsag[dist1 + dist2 + 0]}, {f2tan, f2sag}];
    f2t = f2tan /. fts[[1]];
    f2s = f2sag /. fts[[1]];
```

The answer that we check against is whether or not the second lens matches the one that is input.

```
     ans = Sqrt[f2t*f2s];
     errtab = Join[errtab, {{dist1, ans - lens2}}];
     gooddist1 = Join[gooddist1, {dist1}];
     ];

       If[numreals > 0 && Length[realsols] < 1, d1val = numd1];
    d1val++];
```

Now we find the bounds of the real solutions.

```
If[numreals == 0, attempt = 999, {
    lower = gooddist1[[1]];
    upper = gooddist1[[Length[gooddist1]]];

If[Abs[Plus @@ errtab][[2]]/numreals > thresh && numreals > 1
 && attempt == 1, attempt = 999, {

   If[numreals == 1,
    newdist1tab = Table[i, {i, lower - fac*d1step, upper +
     fac*d1step, d1step/(numstep + 0.1)}],
     newdist1tab = Table[i, {i, lower - fac*d1step, upper +
     fac*d1step, (upper - lower + d1step)/(numstep + 0.1)}]];

     If[Length[errtab] > Length[Select[errtab, #[[2]]
      > 0 &]] &&
      Length[errtab] > Length[Select[errtab, #[[2]] < 0 &]]
        && attempt > 1, zerocross++, If[attempt > 1,
         attempt = 999]];
```

This part of the programme sees if a solution has been found on that particular iteration, and if it has then it finds the solution (where the error crosses through zero).

```
    If[attempt > 1 && zerocross > 0, {
     errfunc = Interpolation[errtab // Sort];
      errsol = FindRoot[ errfunc[d1ans] == 0, {d1ans,
       (errfunc[[1, 1, 1]] + errfunc[[1, 1, 2]])/2}];
errroot = d1ans /. errsol},
      errroot = 0];
    }];
}];
attempt++];
```

There is a 'probability' of a solution found which relates to the fact that the error has crossed through zero, or is approaching zero on the boundaries of viable solutions. If it has crossed through zero, then the probability is 100%. If the error is small and yet does not cross zero (with a possibility being that it is a solution and yet due to the number of steps chosen no solution is found), then this number will indicate an approximate likelihood that a solution can be found.

```
minerr = Transpose[Abs[errtab]][[2]] // Min;
solprob = If[100 - minerr > 0, ((100 - minerr)/100)^2*100
 // Round, 0];

If[errroot >  0, {
        Print[""];
        totalsols++\);
        Print["Solution number ", totalsols];
        Print["f1  ", lens1, "  f2  ", lens2, "  d1  ", dist1,
         "  d2  ", dist2, "  d3  ", dtot - dist1 - dist2,
         "  \[Theta]1 ", \[Theta]1*180/\[Pi], "  \[Theta]2  ",
         ArcCos[Sqrt[f2t/f2s]]*180/\[Pi]];
        }];


        If[attempt > 998, {
      Print["  "];
      Print["There is no solution for f1 = ", lens1, "
       and f2 = ", lens2];
      }];

      Print["Probability of solution  ", solprob, "%"];
      Print["   "];
      f2val++];
```

```
f1val++]
```

The difficulty in modematching is relating this second lens back to a real lens. The error is the difference between the real lens (a discrete parameter) and this solution lens which is a continuous variable. The angle of the second lens may be complex since the angle is found from

$$\cos\theta_2 = \sqrt{\frac{f_{2_{tan}}}{f_{2_{sag}}}} \tag{C.2}$$

which gives a complex solution for $f_{2_{tan}} > f_{2_{sag}}$. When this occurs, it implies that the second lens is tilted in the sagittal plane. For small angles, the angle that is found, θ_2, is still approximately valid.

C.3 Diffraction Within a Resonator

The programme used to solve the problem of diffraction inside a resonator makes a few simplifications in order to decrease the computation time. As mentioned, a large Fresnel number $N \gg 1$ is to be avoided. However, this EC is a ring cavity with two focusing mirrors located closely together which yields an $N \sim 150$. The large Fresnel number implies that between the two mirrors, the diffraction effects of the beam are minimal.

The starting point is the solutions provided by the ABCD method. For the ring cavity, a total distance $d_t = d_1 + d_2 + d_3 + d_4 + d_f$ is given. The ABCD matrix can be used to find the optimal separation of the focusing mirrors d_f. For a total cavity length $d_t = 12m$, and a pair of focusing mirrors with $f = 5cm$, the most stable separation is $d_f = 100.424mm$. This then gives the q parameter for the cavity. In a ring cavity, there are two instances when the beam has a flat profile as shown in Figure C.1 a). We can then calculate the beam waist at position A′.

This q parameter result can then be compared with a linear cavity. The linear

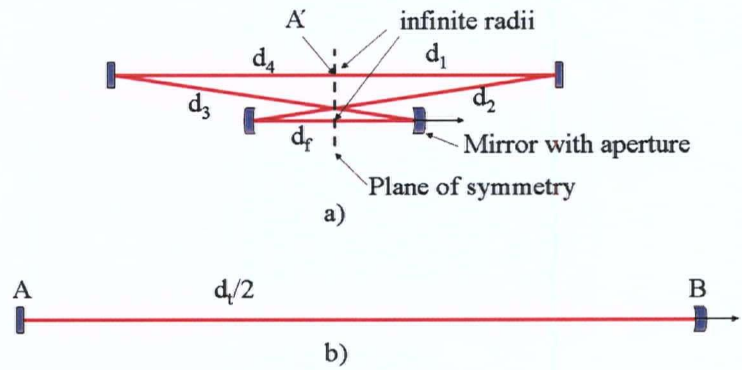

Figure C.1: a)The original ring cavity with identical focusing mirrors and b) the similar linear cavity. The beam parameters are the same for the two cavities at positions A′ and A.

cavity in Figure C.1 b) has the same total cavity length as the ring cavity, and at position A has the same beam waist. Then there is a mirror at B in the linear case which will have the same effect on the beam as the two focusing mirrors in the ring cavity case. It can be shown that the beam spot size on mirror B is the same as on the focusing mirrors. This linear case can have much smaller Fresnel numbers, and so can be computed much quicker. This is the cavity which will be modeled in order to find an appropriate size aperture in the focusing mirrors.

The integral in equation (2.61) has a phase term which is given as

$$\phi_{1,2} = k\left(\frac{Rc_1 - d}{Rc_1}\frac{r_1^2}{2d} + \frac{Rc_2 - d}{Rc_2}\frac{r_2^2}{2d}\right) \tag{C.3}$$

The following code is the integral which needs to be performed until a steady state solution is reached.

```
For[i = 1, i <= imax,
  Print["iteration   ", i]
    (*curved mirror*)
    Print["     Calculating R2"];
```

The fields computed at the mirrors are done discretely, and then interpolated using a built-in routine. The variables `r1` and `r2` are the radial positions along the mirrors A and B with radii `a` and `b` respectively.

```
R2N = Table[{r2, \[ImaginaryI]*k/d*NIntegrate[
 BesselJ[1, k/d*r2*r1]*R1[r1]*r1*
 Exp[-\[ImaginaryI]*\[Phi]1], {r1,0, a}]},
 {r2, h, b + dr, dr}];
R2 = Interpolation[R2N];
R2N = {};
R2Namp = Table[{r2, (Abs[R2[r2]])^2}, {r2, h, b + dr, dr}];
R2amp = Interpolation[R2Namp];
R2Namp = {};
amplitude2 = NIntegrate[x*R2amp[x], {x, h, b}];

(*flat mirror*)
Print["     Calculating R1"];
R1N = Table[{r1, \[ImaginaryI]*k/d*NIntegrate[
        BesselJ[1, k/d*r1*r2]*R2[r2]*r2*
        Exp[-\[ImaginaryI]*\[Phi]2], {r2, h, b}]},
          {r1, 0, a + dr, dr}];
R1 = Interpolation[R1N];
R1N = {};
R1Namp = Table[{r1, (Abs[R1[r1]])^2}, {r1, 0, a + dr, dr}];
R1amp = Interpolation[R1Namp];
R1Namp = {};
amplitude1 = NIntegrate[x*R1amp[x], {x, 0, a}];
```

The lists of amplitudes calculate the power at the mirrors. The relative decrease between iterations is the loss in the cavity due to finite mirror size and the aperture. This is the value that is to be determined to find the largest aperture possible while maintaining a low cavity loss.

```
tabamp2 = Join[tabamp2, {amplitude2}];
tabamp1 = Join[tabamp1, {amplitude1}];
If[i > 2, {
 num = Length[tabamp2] - 2;
    amptab1 = Table[tabamp1[[i + 1]]/tabamp1[[i]],
     {i, 1, Length[tabamp1] - 2}];}];

i++;]
```

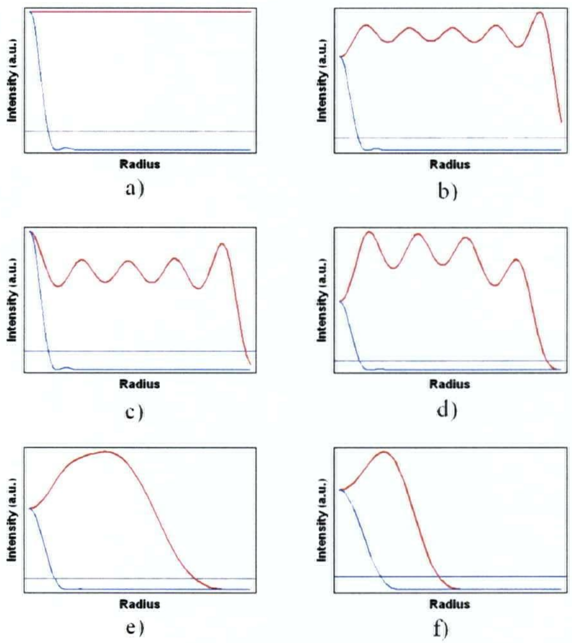

Figure C.2: The diffraction of the beam inside of a confocal resonator with Fresnel number of 5.0. An initially flat profile is given in (a) in red; (b) after 1 iteration; (c) after 5; (d) after 200; (e) after 2000 and (f) after 20 000 iterations. This demonstrates that for the confocal case with large enough Fresnel number, this is a very slow routine to converge to the steady state solution. After 50 iterations, the loss becomes negligible, preventing the convergence.

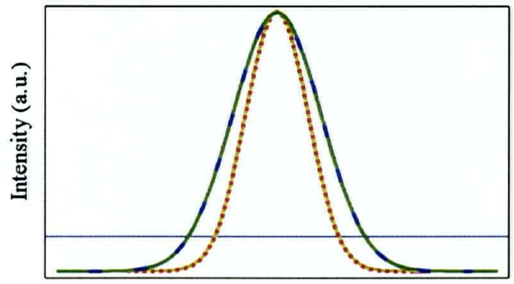

a)

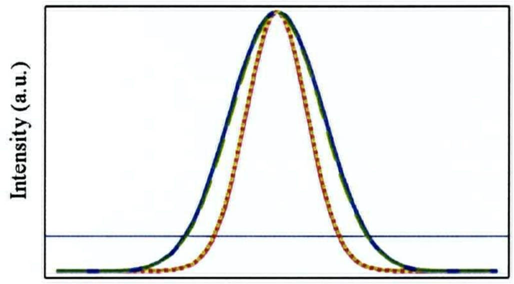

b)

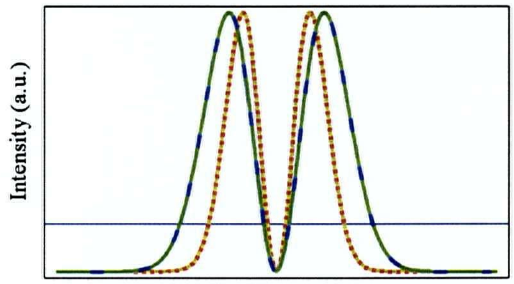

c)

Figure C.3: The beam profile inside the ring resonator calculated at points A (inner curves) and B (outer curves) in Figure C.1. The dotted and dashed lines are the profiles for a stable cavity assuming a gaussian profile (with the waist found at the horizontal line), while the solid lines are those calculated using the Fox-Li method. Notice that in b) the blue curve is wider, avoiding the losses of the aperture. In c) it is a TEM_{10} mode which has no intensity in the middle, and so the aperture has negligible effect on the profile (and loss). The attenuation γ_n per roundtrip in the cavity are as follows: no aperture TEM_{00} – 0.999997; $100\mu m$ aperture TEM_{00} – 0.998363, no aperture TEM_{10} – 0.999999, $100\mu m$ aperture TEM_{10} – 0.999997 (not shown).